JOURNAL OF GEOPHYSICAL RESEARCH, VOL. 86, NO. A10, PAGES 8319-8342, SEPTEMBER 30, 1981

Positive Ion Observations in the Middle Magnetosphere of Jupiter

R. L. McNUTT, JR., J. W. BELCHER, AND H. S. BRIDGE

Department of Physics and Center for Space Research, Massachusetts Institute of Technology Cambridge, Massachusetts 02139

We consider the positive ion data gathered by the Voyager Plasma Science experiment in the middle magnetosphere of Jupiter. The experiment measures positive ions with energies per charge between 10 and 5950 V. The observations are analyzed to obtain the mass and charge densities, velocity components, and temperatures of the low-energy plasma population. The reduced data set is discussed in the context of the outstanding questions concerning this plasma population and its dynamics. We find that on the dayside, there exists a transonic to highly supersonic positive ion population which tends to move azimuthally but does not rigidly corotate with the planet. These ions provide the inertia of the magnetospheric plasma inside of ~40 R_J. The mass density is everywhere dominated by heavy ions, and the mass density gradient is consistent with outward diffusion from the Io plasma torus via flux tube interchange. The ions tend to be concentrated in a plasma sheet which is associated with the current sheet inferred from the magnetic field observations. The plasma in the sheet is relatively cool (~20 eV) in comparison with plasma at higher magnetic latitudes (≳100 eV). In addition to the azimuthal flow pattern, we find a local time asymmetry in the data which we interpret as flow away from the current sheet on the dayside and toward the current sheet on the nightside. This dynamic expansion and contraction of the plasma sheet is presumably driven by the asymmetry in the magnetosphere due to the solar wind interaction.

INTRODUCTION

In 1954, *Burke and Franklin* [1955] discovered radio emissions from Jupiter at 22.2 MHz. Subsequently, radio observations at decimetric and decametric wavelengths established that Jupiter had a magnetic field, that the field was roughly dipolar with a symmetry axis tilted about 10° with respect to the rotation axis, and that the surface equatorial field strength was between 1 and 10 G. The first attempts to model the Jovian magnetosphere used these magnetic field parameters in conjunction with extrapolations of knowledge of the earth's magnetosphere and of the solar wind at 1 AU. *Brice and Ioannidis* [1970] estimated that the distance to the subsolar magnetopause at Jupiter should be ~50 R_J (Jovian radii, 1 R_J is taken to be 71,372 km in this work). At the same time they recognized that the Jovian magnetosphere must be inherently different from that of the earth. In Jupiter's magnetosphere these authors found that the plasmapause and magnetopause should essentially coincide. As a result, Jupiter's magnetic flux tubes should remain full of any plasma created within the Jovian magnetosphere, and the plasma should corotate with the planet [*Davis*, 1947, 1948].

The first in situ measurements at Jupiter were made by Pioneer 10 and 11 in 1973 and 1974. The most striking global discovery was the inflation of the outer magnetosphere to double the expected size. In addition, Pioneer 10 made the unanticipated discovery that outside of 10 R_J a significantly nondipolar magnetic field exists with radially distended field lines. The field distortions were interpreted as being due to the presence of an annular current sheet, warped but rotating rigidly with the planet. The sheet was postulated to be due to the centrifugal forces acting on the low-energy magnetospheric plasma [*Smith et al.*, 1974]. The energetic particle experiments measured regular omnidirectional flux variations near the current sheet defined by the magnetic field observations. The flux maxima were much broader in time than the field minima, and the maxima were best described by a magnetodisc [*Van Allen et al.*, 1974] of quasi-trapped energetic particles aligned with the magnetic dipole equator (that plane passing through the planet, perpendicular to the planetary dipole moment). *Van Allen et al.* [1974] also attributed the field distension to corotating low-energy plasma, with plasma, field, and high-energy particles all symmetric about the magnetic dipole equatorial plane.

Direct measurements of the low-energy positive ions at Jupiter were made by the Pioneer 10 and 11 plasma instrument [*Frank et al.*, 1976]. This instrument measured the energy per charge spectra of positive ions from 100 to 4.8 kV. Assuming that the signal was due to protons, *Frank et al.* [1976] fit subsonic Maxwellian distributions to the spectra and extracted densities and temperatures for the inner regions of the magnetosphere. These authors reported densities from 10 to 100 cm^{-3} and temperatures of the order of 100 eV. The Pioneer observations have been subsequently discussed in the context of a plasma consisting of heavy ions from Io by *Hill and Michel* [1976], *Neugebauer and Eviatar* [1976], and *Goertz and Thomsen* [1979].

In addition to direct measurements of the low-energy plasma in the inner magnetosphere, a number of investigators tried to deduce by indirect means the properties of the more rarefied plasma in the middle and outer magnetosphere [e.g., *Goldstein*, 1977; *Goertz*, 1979; *Walker et al.*, 1978]. The thrust of these modeling efforts was to infer properties of the low-energy plasma from properties of the magnetic field measurements on Pioneer. Such models produced estimates of mass densities and temperatures in the current sheet, with the various temperature estimates ranging from ~1 keV to much greater than 10 keV.

Just prior to the Pioneer 10 encounter, *Brown and Chaffee* [1974] reported observations of neutral sodium associated with Io. This observation was followed by the discovery of a partial torus of singly ionized sulfur associated with Io [*Kupo et al.*, 1976]. These ground-based observations suggested the possibility of a Jovian plasma population dominated by heavy ions. They also underscored the need for a more complete set of in situ measurements of the magnetospheric plasma at Jupiter. Observations made by the Voyager complement of par-

Paper number 80A1602.
0148-0227/81/080A-1602$01.00

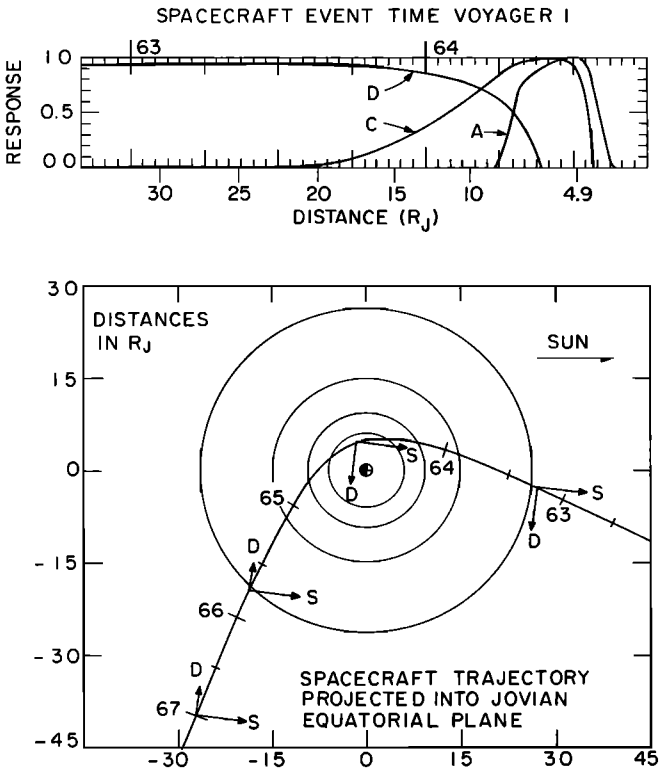

Fig. 1. The Voyager 1 trajectory projected onto the Jovian equatorial plane. The arrow labeled *S* is the projection of the symmetry axis of the main cluster of Faraday cups onto the equatorial plane, and the arrow labeled *D* is the projection of the D cup axis. On the inbound leg the A and D cup axes are essentially in the Jovian equatorial plane, with the B and C cup axes inclined ~17° south and north of that plane, respectively. Tick marks are shown every 12 hours, with day of year at the beginning of the day. The orbits of the four Galilean satellites are also shown. The top panel shows the response of three of the sensors to a cold, corotating beam, as a function of time along the trajectory. Closest approach is at 4.9 R_J (1204 UT on DOY 64, 1979).

ticle and field experiments have dramatically increased our knowledge of the characteristics of this plasma. In the present paper we discuss the positive ion measurements obtained by the Plasma Science experiment in the middle magnetosphere of Jupiter (i.e., from ~10 to ~40 R_J).

Instrumentation and Spacecraft Trajectory

The Plasma Science (PLS) instrument has been described in detail [*Bridge et al.*, 1977], and only salient points are summarized here. The experiment consists of four modulated grid Faraday cups and the associated electronics package. Three of the cups are arranged in a symmetric configuration to form the main sensor. The symmetry axis parallels that of the high-gain antenna, which is locked on the earth except for short intervals during some spacecraft maneuvers. The normals of the main sensor Faraday cups (A, B, and C cups) are tilted at 20° to the symmetry axis and equally spaced 120° in azimuth about it. The side sensor (D cup) normal is tilted 90° to the symmetry axis and located 167° in azimuth from the A cup normal. Looking into the cups, A, B, and C are labeled in a clockwise sense. In what follows, we shall use the terms cup axis, cup normal, and cup look direction interchangeably.

All four Faraday cups measure electric currents from positive ions in the energy per charge range of 10–5950 V. In addition, the side sensor measures currents from electrons. The PLS electron measurements in the magnetosphere are discussed in a companion paper [*Scudder et al.*, this issue]. Measurements are made in a set of contiguous voltage windows whose widths, to first order, increase linearly with voltage. Two positive ion measurement modes are available and have been used in our analysis. The low-resolution mode (*L* mode) uses 16 voltage windows with an energy per charge resolution of ≃29%. The high-resolution mode (*M* mode) uses 128 voltage windows with an energy per charge resolution of ≃3.6%. During the encounter, a complete measurement in the *L* mode takes 3.84 s, with consecutive energy per charge spectra in the *L* mode taken 96 s apart. A complete measurement in the *M* mode takes 30.72 s; however, only currents from 72 of the measurement channels are transmitted during each measurement sequence of 96 s. To obtain a full *M* mode spectrum on the ground, it takes two sequence times, or 192 s. The convention used for our analysis is to form a composite spectrum every 192 s in which data in channels 1–56 (10–400 V) from one measurement sequence are combined with data in channels 57–128 (400–5950 V) from the subsequent sequence.

Because of the finite field of view of the various sensors the direction of the cup normals with respect to the bulk plasma motion is of great importance in interpreting the observations. Except for brief periods of spacecraft maneuvers, the spacecraft attitude is fixed in inertial space. In Figure 1 we show the Voyager 1 trajectory as projected onto the Jovian rotational equatorial plane. In Figure 2 the same type of projection is shown for Voyager 2. During the encounters the main sensor symmetry axis (denoted by *S* in the figures) lay almost in Jupiter's equatorial plane. On the inbound passes the side sensor

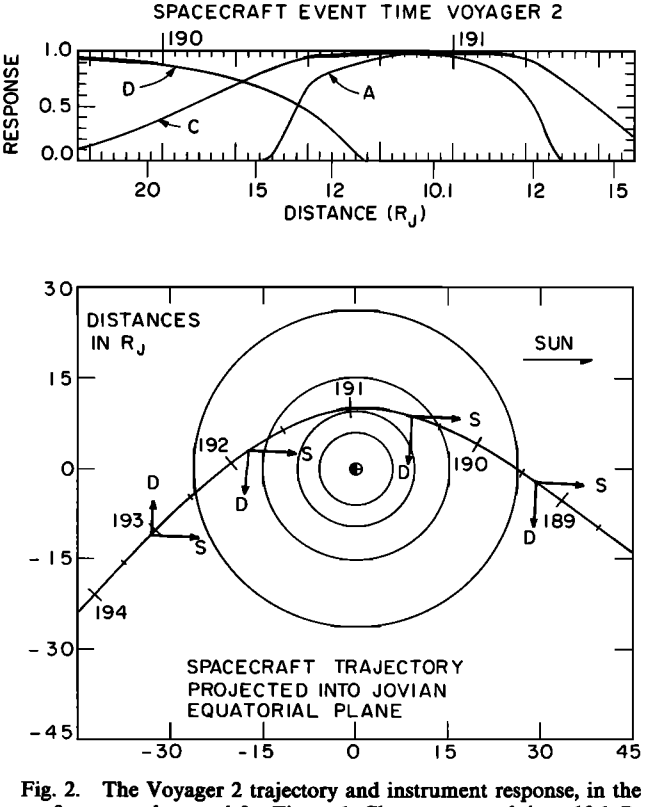

Fig. 2. The Voyager 2 trajectory and instrument response, in the same format as that used for Figure 1. Closest approach is at 10.1 R_J (2230 UT on DOY 190, 1979).

normal (denoted by D in the figures) also lay almost in the same plane. Past periapsis the spacecraft were rolled about the high-gain antenna axis to acquire Arcturus with the Canopus star tracker. In this orientation the normal of the D cup pointed northward of the equatorial plane.

It is qualitatively obvious from the trajectory plots that during the inbound approach to the planet a supersonic plasma flowing azimuthally would be detected primarily by the side sensor and not by the main sensor. As the spacecraft is accelerated around Jupiter, such azimuthal flow would be detected by the main sensor cups near closest approach and then lost to the instrument entirely on the outbound trajectory. These remarks can be made quantitative by considering the sensor responses to a cold rotating beam. The response function of a given sensor is essentially that fraction of a cold beam incident on the aperture which would be measured at the collector (normalized to unity at normal incidence). In Figures 1 and 2 we show the response of the A, C, and D cups to a cold, rigidly corotating beam, including aberration due to spacecraft motion. The response of the B cup closely parallels that of the C cup and is not shown. The B and C cup normals are near–mirror images in the Jovian equatorial plane, pointing to the south and to the north of that plane, respectively, until the change of reference star to Arcturus. Although the Voyager 1 and 2 response curves are qualitatively the same, the D cup response for Voyager 2 falls off earlier prior to closest approach, and the A cup response for Voyager 2 is appreciable for a longer time around closest approach.

AN OVERVIEW OF THE DATA ANALYSIS

The analysis of positive ion data in the middle magnetosphere is a complicated process, and we relegate most of the details of that process to Appendices A and B. A few general comments are in order. The electric currents measured by a Faraday cup are velocity space integrals of the product of the ion distribution function, the component of ion velocity into the cup, and the response function of the sensor. Our present data analysis procedure is limited to those situations in which we can sensibly assume that the response function is near unity over the region of velocity space in which $f(\mathbf{v})$ is appreciable. On the inbound trajectories this assumption is usually good for at least one of the four Voyager PLS sensors (for example, the D cup in the middle magnetosphere). For that sensor we can obtain a simple analytic relation between the measured currents and the plasma parameters describing the positive ion distribution functions, e.g., composition, density, temperature, and (in the case of a single sensor) that component of velocity along the sensor look direction (see Appendix A). With such an analytic relation, least squares determination of the plasma parameters from the measured currents is straightforward, although complicated by the fact that the Jovian magnetospheric plasma consists of an admixture of many ionic species. All of the quantitative plasma parameters in the present paper are based on single-sensor analysis. In particular, we will obtain quantitative velocity estimates only for that component of velocity along the sensor normal.

At the outset we emphasize that our main interest is in the fluid parameters of the plasma—that is, total mass densities, pressures, and velocity components. We are not primarily concerned here with the detailed composition of the plasma (see *Bagenal and Sullivan* [this issue] and Appendix B for details of the composition). However, it is precisely the multispecies composition of the Jovian magnetosphere which makes the data analysis difficult. In terms of mass density, the dominant ionic species in the middle magnetosphere are O^{2+}, S^{3+}, O^+, and S^{2+}, and perhaps S^+. A Faraday cup is an electrostatic device and thus measures the energy per charge distribution of the positive ions. For a plasma consisting of cold ions with a common velocity, the various ionic species will be separated in energy per charge according to their mass to charge ratios. A cold ionic species with mass number A and charge number Z^* will appear at an energy per charge of A/Z^* times the energy per charge of H^+. Thus O^{2+} will appear a factor of 8 above H^+ in energy per charge, S^{3+} a factor of $10\frac{2}{3}$ above H^+, O^+ and S^{2+} a factor of 16 above H^+, and S^+ a factor of 32 above H^+. We obtain maximum information from the Faraday cup measurements when the ions are sufficiently cold to allow the resolution of these various peaks in A/Z^* (i.e., $\gtrsim$Mach 6 for the heavy ion peaks at 8, $10\frac{2}{3}$, and 16 and $\gtrsim$Mach 2 for the separation of the H^+ peak from the heavy ions (see Appendix A)). Figure 3 is one of our best examples of a cold M mode spectrum with excellent species resolution. Peaks at values of A/Z^* of 1, 8, $10\frac{2}{3}$, and 16 are clearly evident. For such spectra we can obtain from our least squares fits estimates of the densities, thermal speeds, and velocity components for each species. Appendix B gives examples of such fits.

Unfortunately, the well-resolved M mode spectrum in Figure 3 is the exception rather than the rule. Such cold spectra usually occur in the high-density regions associated with plasma sheet crossings. More usually, the heavy ion species are warm enough that we lose resolution in the various peaks in A/Z^* but not so warm that the energy per charge resolution between the H^+ peak and the heavier peaks is lost. In practice, this means that when the plasma is warmer, it is much more difficult to determine the densities, thermal speeds, and velocity components of the heavier ions. In principle, we can still derive an accurate value of the velocity component from the H^+ peak. Unfortunately, because of the constant $\Delta E/E$ energy width of the instrument measurement channels the energy per charge windows of the M mode are very narrow at

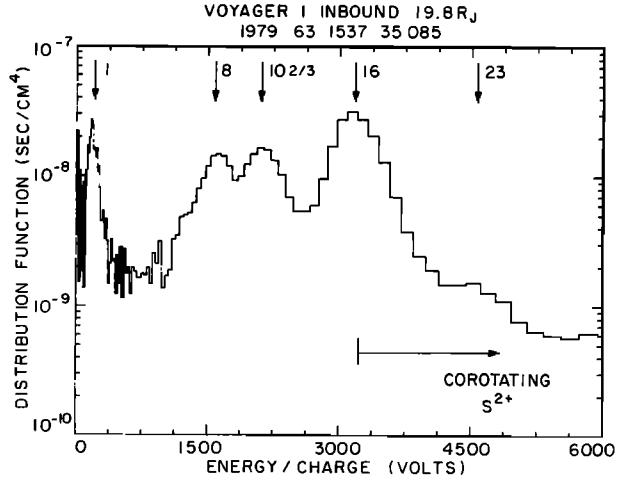

Fig. 3. A high-resolution M mode measurement of the positive ion distribution function at 19.8 R_J from the D sensor. A least squares fit to the 8, $10\frac{2}{3}$, and 16 peaks yields a common velocity component of 195 km/s into the D sensor, and this velocity is used to draw the various arrows in the figure. The velocity component expected on the basis of rigid corotation is 238 km/s. The energy per charge of an S^{2+} ion moving at this speed is also indicated.

low energies, where the H^+ peak is located. As a result, outside of ~15 R_J the signal-to-noise ratio is sufficiently poor in the M mode that the H^+ peak is usually in the noise, although the heavier species, at higher energies and thus wider energy per charge windows, are still well above noise. They are usually unresolved, however, and without the H^+ peak it is impossible to separate out in a quantitative fashion the various A/Z^* values which comprise the unresolved heavy peaks.

The low-resolution L mode, with its much wider energy per charge windows, turns out to be invaluable in this respect. Figure 4 is an example of an L mode spectrum taken just after the M mode spectrum of Figure 3. The wider channel widths at the lower energies improve the signal-to-noise ratio, and frequently throughout the middle magnetosphere the H^+ peak is well above noise and well separated from the heavy peak. In such a situation we can obtain an estimate of the H^+ velocity component into the sensor and thereby a reasonable estimate of the mass density of the unresolved heavy peaks. From our fits we can also derive a quantitative temperature estimate from the H^+ peak, which we find is a good index to the temperature of the heavier ions (Appendix B). Thus although the H^+ ion will turn out to be negligible in terms of the overall magnetospheric dynamics, its presence is important in our analysis, because it is well separated in energy per charge from all other major ions in the Jovian magnetosphere. However, even in the L mode the H^+ peak is frequently not distinct enough for quantitative analysis. For L mode spectra with no distinct proton peak we can obtain little quantitative information other than an estimate of the total charge density of positive ions (see below). However, we will draw many qualitative conclusions from such spectra.

As a final comment, we note that to obtain all three components of the plasma velocity, we must use information from at least three sensors. In the dayside middle magnetosphere, all sensors except the D sensor are usually significantly oblique to the flow. Thus vector velocities can only be obtained using an analysis based on the response for ions which arrive at large angles to the detector normals. The numerical methods required for a multisensor analysis using the full response are well understood in principle, but they are much more complex to implement than the single-sensor analysis we present here. At present, we cannot quantitatively include in our analysis data from sensors whose normals are significantly oblique to the flow, although we hope to analyze such data in the future. In particular, we frequently have substantial signals in these oblique sensors, and there is a large amount of information to be gained from the analysis of these data. To illustrate this point, we will later take advantage of the symmetry properties of the B and C sensors with respect to the Jovian equatorial plane to obtain some qualitative results about the plasma velocity component perpendicular to that plane.

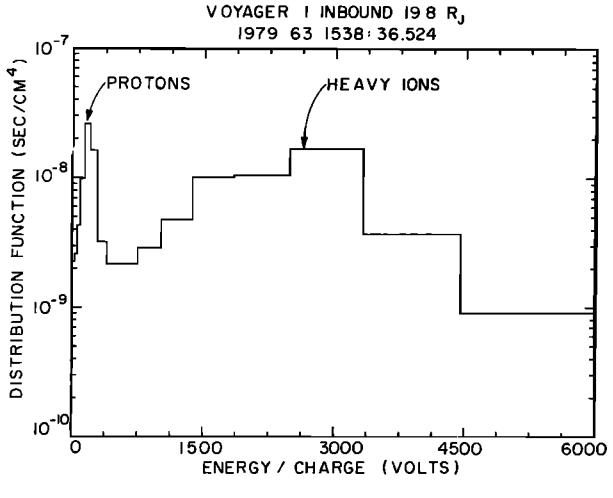

Fig. 4. A low-resolution L mode measurement of the positive ion distribution function at 19.8 R_J from the D sensor. This spectrum was taken just after the M mode spectrum shown in Figure 3.

Plasma Observations in the Middle Magnetosphere

Azimuthal Flow

Bridge et al. [1979*a*, *b*] report that the low-energy plasma in the Jovian magnetosphere tends to move azimuthally about Jupiter. This statement is based on the observation that the relative magnitudes of the positive ion fluxes in the different sensors during the encounters correspond qualitatively to those expected for a cold corotating beam (Figures 1 and 2). For example, in the Voyager 2 encounter, the fluxes in the D cup were larger than those in the main sensors until ~0600 UT on DOY 190 (day of year 190; January 1 is DOY 1), 1979, but thereafter they declined in magnitude compared to those in the B and C sensors. Near closest approach, the relative fluxes in the main sensors varied roughly in the manner one would predict on the basis of Figure 2, with the fluxes in the B and C cups coming up earlier than those in the A cup and the A cup fluxes declining later.

An example of this behavior is shown in Figure 5. This is a positive ion spectrum in the L mode obtained by Voyager 2 on DOY 189 at 2250 UT, when the spacecraft was 20 R_J from Jupiter. Rigidly corotating flow at this distance would appear at a speed of 240 km/s, with the aberrated flow velocity at angles of 95°, 69°, 64°, and 19° to the A, B, C, and D cup axes, respectively (0° is directly into the cup). Thus we would expect to see corotating H^+ (O^{2+}) at an energy per charge of ~300 V (~2400 V) in the D cup and at an energy per charge of ~75 V (~600 V) in the B and C cups. The positive ion spectra in the B, C, and D cups in Figure 5 are consistent with the unresolved presence of H^+ plus heavy ions at roughly these energies. The low-energy shoulder in the D cup is probably H^+, with the higher-energy peak due to heavy ions. In the B and C cups the H^+ shoulder disappears because of projection effects, and the heavy ion peak moves to lower energies and also lower fluxes because of the cup response. For a cold beam the A cup should show no response at this time, and thus the fluxes in the A cup must be due to the finite thermal spread of the beam. We note that the energy per charge limit of 5950 V for the PLS observations refers to normal incidence. For oblique incidence the detectors respond to much higher energies, albeit at a reduced level. For example, in the present case a corotating ion with an energy per charge of 30 kV would not appear at all in the D cup spectra but would appear in the highest channel of spectra in the B and C cups. There may be some indication in Figure 5 of very heavy ionic species in the B and C cup spectra at higher energies per charge (e.g., at mass to charge ratios of 32, 64, or higher [see *Sullivan and Bagenal*, 1979]). Such signals may also be due to a very hot component of the plasma, as discussed by *Krimigis et al.* [1979] (see also *Belcher et al.* [1980]).

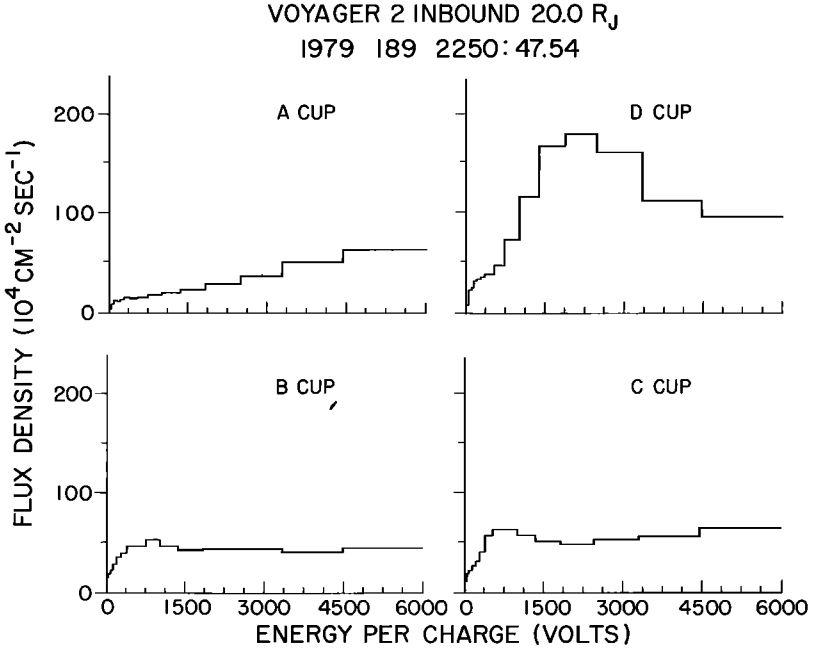

Fig. 5. The flux density of positive ion charge, in units of proton charges per square centimeter per second, versus energy per charge for an L mode measurement from Voyager 2.

Qualitatively, it is clear from these spectra that at this distance the positive ions are reasonably supersonic and moving azimuthally to first order (radial and vertical motions also occur, as we discuss below, although in general these are second-order effects). This general pattern holds throughout both the Voyager 1 and the Voyager 2 encounters. For future reference, we note that the equal flux levels in the B and C sensors in Figure 5 suggest that the vector velocity is more or less in the Jovian equatorial plane at this time, since the B and C sensors are symmetrically oriented south and north with respect to that plane.

The Charge Density of Positive Ions

The D cup spectrum in Figure 5 is representative of ~70% or more of the L mode spectra obtained during the Voyager 1 encounter. As we discuss in subsequent sections, the remaining 30% of the L mode spectra from Voyager 1 display a distinct separation between H^+ and the heavy ions and can be analyzed in some depth for temperatures, mass densities, and velocity components. In contrast, the only quantitative parameter that we can derive from spectra such as those shown in Figure 5 is the total charge density of positive ions in the PLS energy per charge range. For example, the total flux density of positive ion charge in the D cup spectrum of Figure 5 is 1.1×10^7 proton charges per square centimeter per second. This flux density is the product of the total positive charge density in this range, N_+, times the (common) ion velocity component in the cup, V_n (see equation (15) of Appendix A). Thus if we assume that V_n is 200 km/s at this time, N_+ must be 0.54 proton charges per cubic centimeter. Given an estimate of V_n, we can transform total flux density measurements to estimates of N_+ with no assumptions as to composition.

We now proceed to display the flux density measurements from Voyager 1 and 2 in this form. We show the number density calculated from measured flux densities in the sensor with the greatest response to a cold corotating beam (i.e., for Voyager 2 the D cup before ~0630 UT on DOY 190, the C cup between ~0630 and ~2030 UT, etc.). For our estimate of V_n we assume that the plasma rigidly corotates with the planet inside of 17.5 R_J, and we take V_n to be the appropriate component of corotational velocity (compensated for the effects of spacecraft motion). Outside of 17.5 R_J the D cup is always the cup with maximum response to corotation, and here we assume that V_n is constant at 200 km/s. This velocity model is in reasonable agreement with the results we will obtain below from our fit procedures.

The values of N_+ so obtained are shown as a function of time in Figure 6 for Voyager 1. We also indicate in this figure the radial distance of the spacecraft from the planet and the distance of the spacecraft above the magnetic equatorial plane. In order to easily compare variations in plasma properties from the inner to the middle magnetosphere we show in Figure 6 data from 4.9 to ~40 R_J. The charge density is everywhere derived from the analysis described above. The mass density is from the fits described below outside of ~10 R_J and from the fits of *Bagenal and Sullivan* [this issue] inside of ~10 R_J.

The charge density profile for Voyager 1 is, of course, dominated by the Io plasma torus, as discussed in detail by *Bagenal and Sullivan* [this issue]. The density decreases rapidly as we move into the middle magnetosphere. Globally, the charge density in the middle magnetosphere shows two local increases every Jovian rotation period (9 hours 55 min) except for the increases centered at the beginning of DOY 64. The local maxima are located near crossings of the magnetic dipole equatorial plane. This is in agreement with the magnetodisc interpretation of the Pioneer field and particle data. However, the decreases in magnetic field magnitude [*Ness et al.*, 1979*a*] and increases in plasma density do not always coincide. Hence the term 'magnetodisc' as originally employed [*Van Allen et al.*, 1974] is not fully descriptive of the plasma data. To be precise in our terminology, we will speak of the 'current sheet' in reference to the magnetodisc signature in the mag-

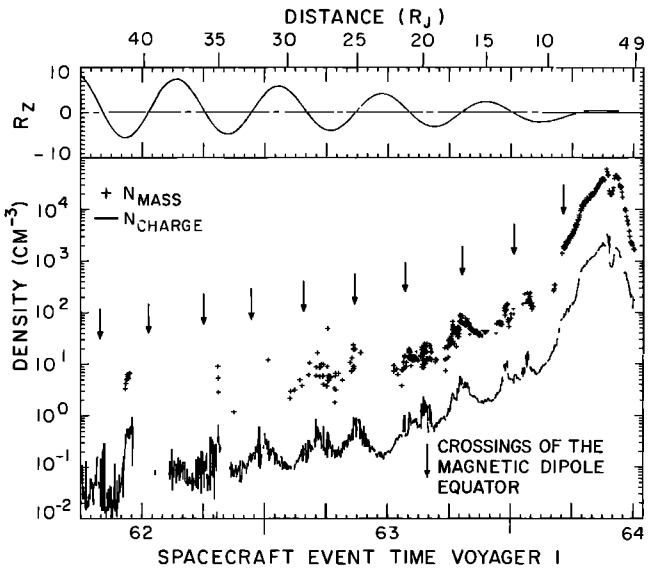

Fig. 6. Estimates of the total mass and charge densities of positive ions, in units of amu per cm^3 and proton charge per cm^3, respectively, for the Voyager 1 encounter. The top panel shows the distance of the spacecraft from the magnetic dipole equatorial plane, and arrows in the bottom panel indicate the crossings of this plane.

netic field data and of the 'plasma sheet' in reference to the signature in the Plasma Science experiment data.

The Voyager 2 data are displayed in a similar manner in Figure 7. The plasma sheet crossings do not show the regular structure seen in the Voyager 1 data. Pronounced crossings are centered at 2230 UT on DOY 188, at 0130 UT on DOY 189, and also at 1200 UT on DOY 189. The abrupt crossings at 2100 UT on DOY 190 and at 0930 UT on DOY 191 are also clearly defined, unlike the density enhancement centered at 2230 UT on DOY 189. The Ganymede wake phenomenon is readily apparent from 0400 to 1200 UT on DOY 190 [*Bridge et al.*, 1979*b*; *Burlaga et al.*, 1980] and tends to obscure any regular density increases in this region.

In terms of systematic errors the estimates of N_+ in Figures 6 and 7 will (1) underestimate the density for supersonic plasmas, with an error which goes as the inverse square of the Mach number, (2) underestimate the density because we assume unit response when, in fact, the response is sometimes significantly less than unity (in particular, on DOY 64 near 0430 UT for Voyager 1 and on DOY 190 near 0630 UT for Voyager 2, when corotating flow is moving out of the field of view of the D sensor and into the field of view of the C sensor) (3) underestimate the density at large distances because of those heavy ions which fall outside of the PLS energy range (e.g., S^+ at 200 km/s has as an energy per charge of 6681 V) (4) overestimate the density if we have underestimated the velocity V_n outside of 17.5 R_J. Errors due to point 1 are at the 10–20% level for Mach numbers of 2–3, which appear to be a reasonable lower limit for the Mach numbers of the heavy ions. Errors due to point 2 are larger than this at times but can be qualitatively estimated from the cold responses given in Figures 1 and 2. Errors due to points 3 and 4 are harder to estimate, but they tend to compensate for each other. For example, the major contributors to N_+ in the middle magnetosphere have mass to charge ratios of 8, 10⅔, and 16. An ion with a mass to change ratio of 16 moving at 200 km/s has an energy per charge of 3340 V, within the PLS range. At 300 km/s, however, it is above the PLS energy range at 7516 V. Thus if the ions in an unresolved D cup spectrum at ~30 R_J are actually moving at 300 km/s instead of our assumed 200 km/s, the measured flux density will be low because the 16 peak is above the PLS range. However, we tend to compensate for this by dividing the measured flux density by the (hypothetically) low value for V_n of 200 km/s. Thus the cumulative error in N_+ is probably no more than a factor of 2 in the range from 20 to 40 R_J. Inside of 20 R_J the error should be less than 20–30% and should be decreasing with distance, since the velocities are more nearly corotational and the major ionic species are inside of the PLS energy per charge range.

The PLS electron measurements offer independent support for this determination of N_+. Estimates of the electron densities agree with the ion charge densities in Figures 6 and 7 at a 30% level over a range of densities from 3×10^{-2} cm^{-3} to 100 cm^{-3} for Voyager 1 [*Scudder et al.*, this issue]. For densities below 3×10^{-2} cm^{-3}, our estimates of N_+ tend to be preferentially higher than the electron density estimates. The positive ion measurements at these low densities may be affected by electron leakage. This effect is most serious when a substantial fraction of the electron population is above the 90-V suppressor voltage of the positive ion mode [*Olbert*, 1968]. This fraction of the electron population is modulated to some extent, producing an ac signal which adds to the positive ion signal. Because the electrons in low-density regions of the magnetosphere are hot, with characteristic temperatures of keV, the leakage effect is potentially more serious in such regions. At higher densities, as discussed by *Scudder et al.* [this issue], the electron population is increasingly dominated in number by a cold component with characteristic temperatures of 100 eV and less, and the fraction of electrons above 90 V is correspondingly decreased. Preliminary estimates of this leakage effect based on the observed electron spectra indicate that leakage may affect the positive ion densities at the 10^{-2} cm^{-3} level (S. Olbert, private communication, 1980). At higher densities the cooler electron population has little effect on the positive ion measurements.

For Voyager 2 we show in Figure 8 a comparison of the electron and positive ion charge densities between 10.1 and 22

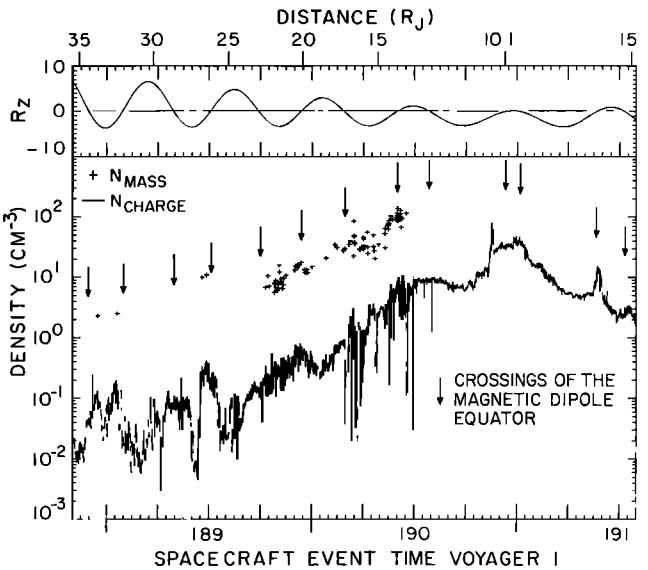

Fig. 7. Estimates of the mass and charge densities of positive ions for the Voyager 2 encounter.

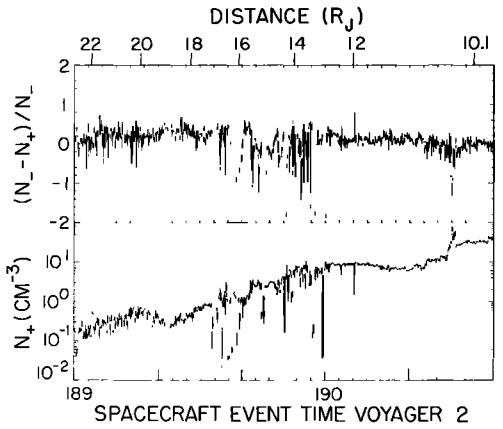

Fig. 8. A comparison of the PLS electron (N_-) and positive ion (N_+) charge densities from 10 to 22 R_J on Voyager 2.

R_J. With the exception of the Ganymede wake region and the plasma sheet crossing at 2100 UT on DOY 190, the agreement between the positive and negative charge densities is at worst at the 30% level and at best (near closest approach) at the 10% level. It is hard to evaluate the significance of the larger disagreements in the Ganymede wake region because of severe time aliasing problems, with variations in the density estimates by as much as a factor of 100 within 96 s. In the cold, high-density region near 2100 UT on DOY 190 the electron analysis is complicated by the presence of a negative spacecraft potential of order 10 V, which leads to an underestimate of N_-. A similar problem in the interpretation of the electron data is encountered in the dense, cold plasma of the Io torus on Voyager 1, as discussed by *Scudder et al.* [this issue]. Outside of these regions the good agreement in the total negative and positive charge densities supports the validity of both determinations. It is worth noting that these estimates of the total charge density were obtained independently by two different data analysis groups with no subsequent adjustment of either data set to improve the agreement shown in Figure 8. The scatter in Figure 8 is not due to random errors in the analysis. As will become more apparent below, the scatter reflects actual changes in the density by substantial percentages on time scales of 96 s and less. Thus the comparison between electron and positive ion densities is complicated by the fact that these observations are taken at different times in the 96 s measurement cycle.

Finally, we note that there is an embarrassment of riches in terms of the positive ion charge density during the Voyager 2 encounter. A comparison of the charge densities in Figure 7 with those determined by the low-energy charged particle experiment (LECP) as presented by *Gurnett et al.* [this issue], assuming doubly ionized oxygen, demonstrates that both experiments frequently account for almost all of the available electron density. For example, consider the Voyager 2 encounter near closest approach. *Gurnett et al.* [this issue] quote an electron density determined from upper hybrid resonance emissions of 29–52 cm^{-3} at 0010 UT on DOY 191, near 10 R_J. The electron density determined by PLS at this time is ~39 cm^{-3} [*Scudder et al.*, this issue]. The positive ion charge density determined by the LECP experiment for oxygen ions with energies greater than 66 keV, assuming O^{2+}, is ~32 cm^{-3} [*Krimigis et al.*, this issue]. The positive ion charge density determined by PLS for ions with energies per charge below 6 kV is ~36 cm^{-3}. Since we are including no charge density due to ions between 6 and 66 keV, charge neutrality requires that at least one of these estimates of charge density be in error by a factor of order unity.

In defense of the PLS determination of N_+ we emphasize that we have made no assumptions as to charge state or composition. The PLS determination is based on a direct measure of the total charge flux density of positive ions in the energy per charge range of the instrument. If the plasma flows supersonically into a given sensor, the charge density of ions in the PLS energy range can be obtained by dividing this flux density by the common ion velocity component into the sensor (the A cup in the case of Voyager 2 at the beginning of DOY 191). Examination of the positive ion spectra in the A cup at this time shows the plausible presence of O^{2+}, S^{3+}, S^{2+} or O^+, and S^+ moving supersonically (Mach numbers of ~4) and appearing near the energies per charge expected for rigid corotation. Our estimate of V_m, assuming rigid corotation, is a reasonable one at ~10 R_J. In terms of absolute calibration we note that the PLS total positive ion densities in the Io torus show excellent agreement with the planetary radio astronomy (PRA) determinations [*Bagenal and Sullivan*, this issue]. For example, near 0925 UT on DOY 64 the PRA determination of N_- is ~3520 cm^{-3} [*Warwick et al.*, 1979]; the PLS determination from an *M* mode spectrum at 0925 UT, using the above technique, is 3300 cm^{-3}. This is only one of many checks of the accuracy of the PLS calibration. Overall, we estimate that our determination of the Voyager 2 ion charge densities near closest approach (in the PLS energy range) is in error by no more than 15%. The majority of the positive ion charge density which balances the electron charge density lies below 6 kV at this time.

Global Plasma Parameters From Least Squares Fits

Although the positive ion charge density is of great interest, other quantities (such as the mass density and ion temperature) are of more importance in determining magnetospheric dynamics. We can only obtain information about such quantities from least squares fits to resolved ion spectra. The great variability of the data with respect to temperature, composition, and signal-to-noise ratio precludes fitting all dayside middle magntosphere data with the same level of confidence. The greatest information content is in the resolved *M* mode spectra, which give the most reliable estimates of the plasma parameters. In order to obtain the best velocity component values we have included in our global study only those *M* mode spectra with at least two clearly resolved peaks in the heavy ions (usually $10\frac{2}{3}$ and 16). We searched through both the Voyager 1 and the Voyager 2 *M* mode data sets and found 62 such spectra from the former and only 2 from the latter. In the *M* mode, noise tends to obscure the H^+ signal, so we only fit to the three heavy ion species in those spectra selected for analysis. The three species are assumed to be O^{2+}, S^{3+}, and O^+; to be comoving; and to have independent temperatures.

To extend this limited data base, we have also visually examined all *L* mode spectra obtained in the encounters, selecting only those spectra with a well-defined H^+ peak and a well-defined heavy ion peak (i.e., as in Figure 4). From the Voyager 1 encounter we selected 573 *L* mode spectra for analysis, This represents about 30% of the data taken between the last inbound magnetopause crossing at 0235 UT on DOY 62 [*Bridge et al.*, 1979*a*] and the time at which the proton signal

dropped below our energy per charge scan range at ~0430 UT on DOY 64. The protons drop out because of the decrease in the relative speed between the spacecraft and the plasma near closest approach. Using the same criteria as for the Voyager 1 *L* mode data, we selected 161 Voyager 2 *L* mode spectra for analysis. The smaller number of spectra as compared to the number selected from the Voyager 1 data set reflects the fact that during the Voyager 2 encounter the effective Mach numbers of the various plasma constituents were lower. As a result, fewer spectra are resolved into the H^+ and heavy ion peaks, a resolution which we require for our quantitative analysis. We can draw some qualitative conclusions about upper limits to the temperature for the unresolved *L* mode spectra (i.e., as in Figure 5), but we defer this discussion until after presentation of the quantitative results. On the basis of the fits to the *L* mode data discussed in Appendix B (and many other examples given by *McNutt* [1980]) we choose to fit H^+, S^{3+}, and O^+ to the *L* mode spectra selected for analysis, with S^{3+} and O^+ constrained to have the same temperature. The H^+ temperature is an independent fit parameter, and all species are assumed to be comoving. Other schemes are possible, but this selection seems to give the most consistent and error-free results.

We have applied our nonlinear least squares fit analysis to these selected Voyager 1 and Voyager 2 spectra to obtain values of the mass density, bulk velocity component into the side sensor, and temperature of the plasma in the dayside middle magnetosphere. The mass densities so derived, normalized to the proton mass (i.e., essentially in amu cm^{-3}), from both the *L* and the *M* mode, are shown by the crosses in Figure 6 for Voyager 1 and in Figure 7 for Voyager 2. We emphasize that even though there is an intrinsic ambiguity in the species identification for a given A/Z^* peak (i.e., is the 16 peak S^{2+} or O^{+}?), the total mass and charge density determinations are unaffected by that ambiguity (see Appendix A). For completeness, the Voyager 1 plot contains mass density determinations inside of 10 R_J from the fits of *Bagenal and Sullivan* [this issue]. Comparison with the charge density curve in the Voyager 1 figure shows that the spectra excluded from the analysis tend to lie away from crossings of the plasma sheet. This is consistent with plasma in the sheet being more dense and cooler (see below), resulting in spectra with less noise and better species resolution. The situation is less clear on the Voyager 2 pass, where the plasma sheet crossings are less well defined.

The velocity components as determined from the Voyager 1 *M* mode and *L* mode analyses are shown in Figure 9. We give the components obtained from the *L* mode and the *M* mode analysis separately both to show the respective coverages and because the *M* mode determinations of V_n are more accurate. These data are shown for the same time period as that used in the density plot (Figure 6). Radial distance from Jupiter is shown at the top. We have also plotted the velocity component which would be measured in the side sensor if the plasma were rigidly corotating with the planet. In general, the velocity component lags the corotation value, with the lag increasing with increasing radial distance [*McNutt et al.*, 1979]. Where the results from both the *L* mode and the *M* mode analyses are available, it can be seen that these are in good agreement and show the trend to constant velocity components outside of ~20 R_J. This is the basis for our velocity model used in computing the charge density curves of Figures 6 and 7.

Prior to the Voyager 1 encounter, there was no expectation that the magnetospheric flow would deviate from rigid corotation as close to Jupiter as ~10 R_J. We have been extremely conservative in our selection of spectra for quantitative analysis, at least in part, to establish unequivocally this departure from corotation. Our best estimates of V_n are from fits to the resolved *M* mode spectra such as those given in Figure 3. The

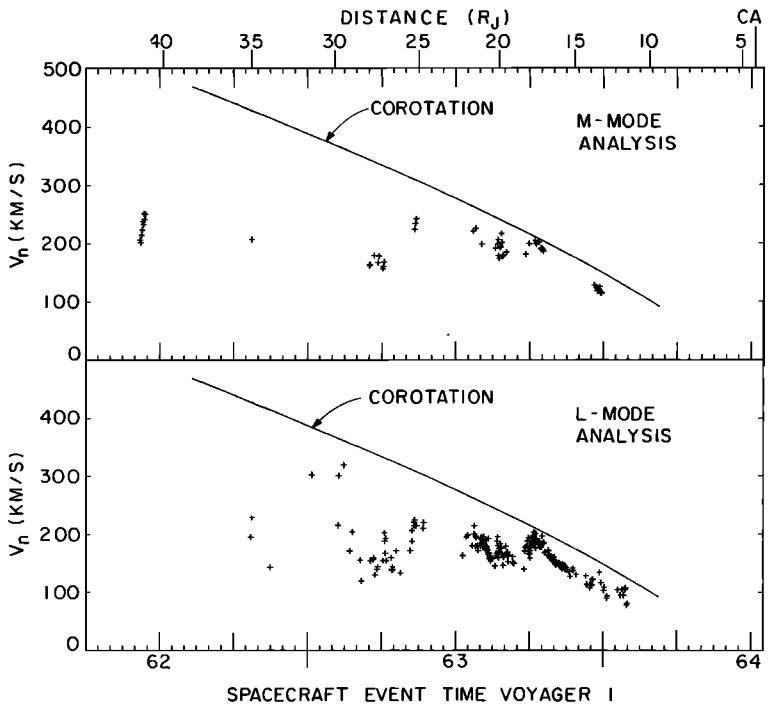

Fig 9. Values of the component of velocity into the D sensor for Voyager 1 as determined from the *M* mode and the *L* mode analysis. The component of velocity into the side sensor expected for rigid corotation is also shown.

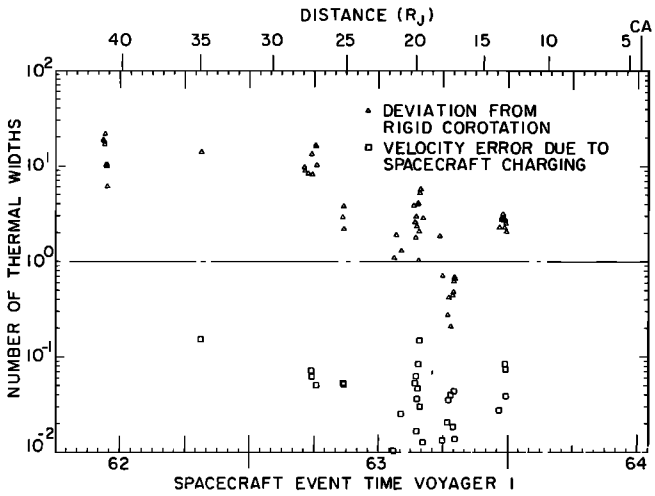

Fig. 10. The triangles indicate the deviation from rigid corotation in the M mode as measured in thermal widths of the 16 peak. In the same units, the squares show upper limits for the error in the velocity estimates due to spacecraft charging.

formal error in these fits is always small (e.g., less than 1 km/s for the fit to the heavy ions in the spectrum in Figure 3). Formal errors are open to interpretation, however. Instead of quoting such errors, we prefer to measure the deviation from corotation for the M modes shown in Figure 9 in units of the thermal width of the O^+ peak. For example, the O^+ peak in Figure 3 has a fit thermal width of 11 km/s. The fit value of V_n is 195 km/s as compared to an expected value of 238 km/s. Thus the O^+ peak in Figure 3 is 3.9 thermal widths below the expected corotation speed. It should be obvious that our determination of V_n is accurate to some fraction of a thermal width (see also *Belcher et al.* [1980]) and that therefore the heavy ions in Figure 3 are not rigidly corotating. This dimensionless measure of the deviation from corotation is shown by the triangles in Figure 10 for the other M mode determinations of V_n. The values range from $\frac{2}{10}$ of a thermal width away from rigid corotation near 1800 UT on DOY 63 to more than 20 thermal widths away near 1030 UT on DOY 62.

We also obtain an upper limit for the error in the M mode determinations of V_n due to possible charging of the spacecraft. We can estimate the spacecraft potential and its effect on V_n as follows. Assume that the spacecraft has acquired a potential $\phi_{s/c}$. Suppose that an ionic species of mass to charge A_i/Z_i^* appears at a measured PLS voltage ϕ_i, corresponding to an apparent velocity V_{ni}, even though in the plasma its true velocity is U_n. Then, clearly,

$$\tfrac{1}{2}A_i m_p V_{ni}^2 = Z_i^* e\phi_i$$

$$\tfrac{1}{2}A_i m_p U_n^2 = Z_i^* e(\phi_i + \phi_{s/c})$$

where m_p is the proton mass and e is the proton charge. If V_{ni} is measured for two different species and U_n is assumed to be the same for both, then we can solve for $\phi_{s/c}$ and the true velocity U_n. In practice, we will obtain the best estimates for $\phi_{s/c}$ by using H^+ and a heavy species. We estimate the uncertainty in the determination of V_n by using our M mode value (based on the heavy ions alone) and an adjacent L mode estimate of the H^+ velocity, based on a fit to the proton peak only. We again express the difference between U_n and V_n in units of the O^+ thermal speed. The absolute value of this ratio is indicated in Figure 10 by the squares. Not all M modes have a quoted error because there is sometimes no adjacent resolved L mode. The upper limit on the error in V_n due to spacecraft potential never exceeds $\frac{2}{10}$ of a thermal width and is usually much lower. Thus we can quantitatively eliminate spacecraft charging as an explanation for the observed departures from corotation on Voyager 1.

The velocity component results from Voyager 2 show similar departures from corotation. We forego the display of the Voyager 2 velocity results until the discussion section below, where we present them in a more useful format. The coverage from both Voyager spacecraft suggests that the lack of rigid rotation may be a permanent characteristic of the middle magnetosphere on the dayside.

The temperatures found from the L mode analysis of H^+ for the Voyager 1 and 2 data are shown in Figures 11 and 12. These figures also contain the O^+ temperature determinations from the M mode spectra (these are generally comparable to the H^+ temperatures). The time periods are the same as those used in the density graphs. For reference, we have used arrows to indicate the location of the crossings of the magnetic dipole equatorial plane. These are also given in the density curves (Figures 6 and 7). In both cases the temperature of the resolved proton component is $\lesssim$200 eV. The Voyager 1 curve shows large local variations, with the temperature decreasing in the plasma sheet crossings. This variation is not so apparent in the Voyager 2 data. Also, the temperature tends to increase slightly with increasing radial distance.

We find that for the Voyager 1 encounter, the resolved M mode spectra generally occur in the regions where the H^+ temperatures, as found from the L mode spectra, show decreases (i.e., in the plasma sheet). This is in keeping with the fact that the individual heavy ions are only resolved at large sonic Mach numbers. The absence of decreases in the Voyager 2 temperature profile for H^+ is consistent with the general absence of resolved M mode spectra in the Voyager 2 data set. Comparing the density profiles (Figures 6 and 7) and the temperature profiles (Figures 11 and 12), it appears that during the inbound pass of Voyager 1, large thermal gradients existed across the plasma sheet, with the low-energy plasma being cooler and much more dense inside the sheet than outside. The Voyager 2 observations show fewer crossings of this nature, especially between ~12 and ~25 R_J. However, there are two plasma sheet crossings on Voyager 2 which do exhibit pronounced temperature/density correlations (DOY 190 at

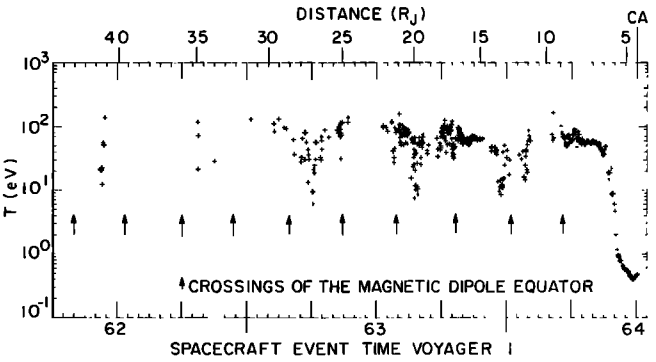

Fig. 11. Outside of 10 R_J we show for Voyager 1 temperature estimates for H^+ (L mode) and for O^+ (M mode) from the present analysis. Inside of 10 R_J the temperature is the total temperature of the ionic species fit by *Bagenal and Sullivan* [this issue], that is, the sum of the individual species temperatures weighted by the number densities.

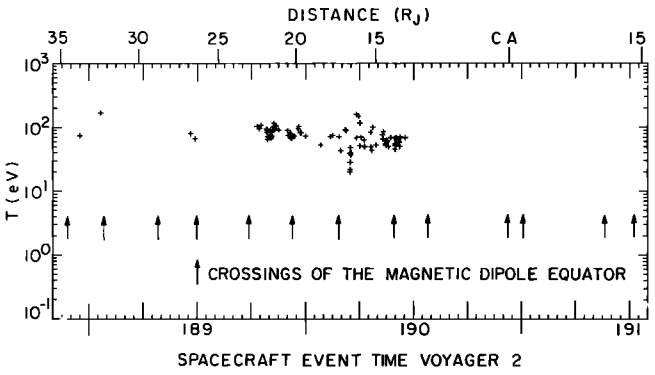

Fig. 12. Temperature estimates for Voyager 2.

~2100 UT and DOY 191 at ~0930 UT), as we discuss in more detail below.

Qualitative Estimates of Temperature

As we pointed out above, we have been conservative in our selection of spectra for quantitative analysis so as to obtain the best estimates of the departures from rigid corotation on the dayside. Gaps in the temperature profiles in Figures 11 and 12 result from a selection effect based on temperature via the effective Mach number. A Mach 1 proton distribution with a bulk speed of 200 km/s has a temperature of about 200 eV and will not be resolved from the heavy ion signature in the L mode (cf. equation (13)). Yet we have selected L mode spectra for analysis on the basis of their having a resolved proton peak. Thus spectra exhibiting higher temperatures than ~100 eV have effectively been eliminated from the data set. To estimate qualitatively the temperature of the ions in the unresolved L mode spectra, we have applied our L mode fit analysis to all spectra in the D cup in the middle magnetosphere, resolved or not. Fits to the unresolved spectra give values for the S^{3+} and O^+ 'temperatures' which are usually below 3 keV. As noted in Appendix B, this temperature estimate in the L mode is always an upper limit because the fit overestimates the heavy ion temperature to account for fluxes due to ionic species known to be present but not included in the fit analysis (e.g., O^{2+}). Where quantitative comparisons with resolved M mode spectra are possible, the L mode estimate of the heavy ion temperatures is typically a factor of 6–10 high. Our qualitative analysis indicates that within 40 R_J of Jupiter the temperature of the magnetospheric plasma in the PLS energy per charge range is typically ~1 keV or less, more probably less. This estimate reflects the fact that in almost all cases the distribution functions of the measured spectra peak below 6 keV, a result which is only consistent with a plasma temperature of less than ~6 keV [see *Belcher et al.*, 1980].

Global Flow Information From Main Sensor Data

In addition to the quantitative least squares fit values of V_n from single-sensor analysis, we also have available more qualitative information about the full vector velocity from multiple-sensor analysis. Figure 13 shows an example of multiple-sensor data from which we can fairly easily derive an estimate of the vector velocity. These spectra were taken at 21.6 R_J inbound on Voyager 2. They occur some 3 hours earlier in time than the spectra shown in Figure 5. In the discussion of Figure 5 we concluded that (1) the flow velocity was mostly azimuthal at the time because the D sensor fluxes were much higher than the fluxes in the main sensor and (2) the flow was in the equatorial plane because of the nearly symmetric orientation of the B and C cups with respect to that plane and because of the near-equality of the fluxes in those cups. In contrast, in Figure 13 the B and C sensor fluxes are comparable to those in the D sensor, even though the sensor orientation is qualitatively the same as the orientation in Figure 5. In consideration of the sensor orientations this fact must imply a component of velocity radially toward the planet during this interval superimposed upon the general azimuthal flow. In addition, the C

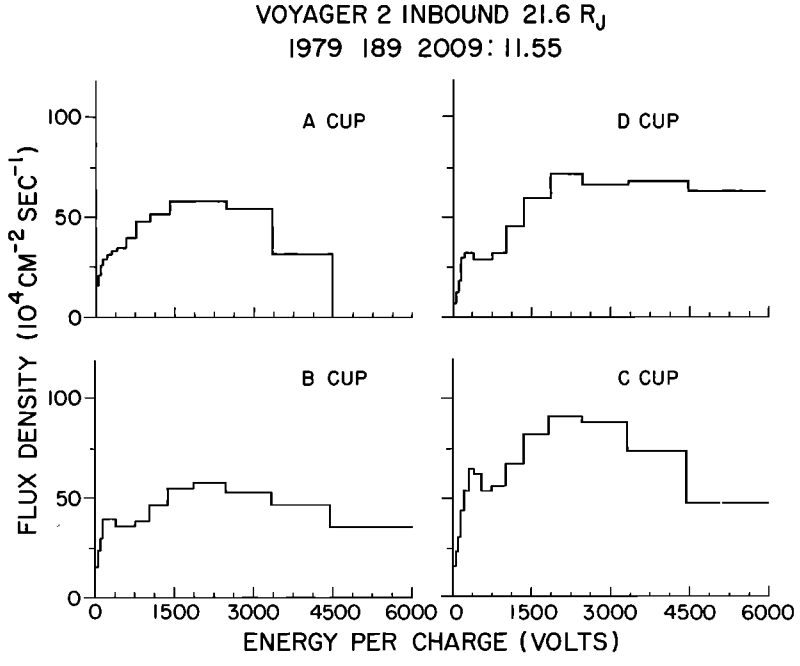

Fig. 13. The flux density of positive ion charge versus energy per charge for an L mode measurement from Voyager 2.

cup fluxes are larger than the B cup fluxes. This inequality has to be interpreted with more caution. In the Canopus orientation the B and C cups are not exactly symmetric with respect to the Jovian equatorial plane. The C cup is slightly closer to corotational flow than the B cup (~67° compared to ~73°) on the inbound leg of both encounters, with the situation reversed outbound. Thus plasma in strict corotation would produce larger fluxes in the C cup than in the B cup on the inbound trajectories, with the opposite situation on the outbound trajectories. However, this difference is too small to account for the inequality of the B and C cup fluxes in Figure 13, as we justify more quantitatively below. Since the C cup is northward looking with respect to the equatorial plane, the obvious conclusion is that the inequality in the B and C cup fluxes is due to a southward component of the flow. Thus Figure 13 is consistent with a vector velocity with a component in the direction of corotation but also significant components southward and radially inward toward the planet. The spacecraft is 3.3 R_J below the magnetic dipole equator at this time. Thus the southward flow is away from the equatorial current sheet.

To put these conclusions on a more quantitative footing, we have analyzed the spectra in Figure 13 with the simulation program used by *Belcher et al.* [this issue] for the interpretation of the PLS data near the Io flux tube. This program was developed by V. M. Vasyliunas, J. D. Sullivan, and one of the authors (J.W.B.) to help interpret data when the full response of the sensors must be used (e.g., for oblique or subsonic flows). The program is sufficiently inefficient at present that it cannot be used to analyze data in a least squares sense, so that we cannot use it for the bulk processing of multisensor data (see the discussion in the paper by *Belcher et al.* [this issue]). However, for individual spectra such as those shown in Figure 13 it can be used in a trial and error mode to produce a reasonable representation of the data. For the H^+ component of these spectra, such an analysis yields a number density of ~0.1 cm^{-3}, a thermal speed of 120 km/s, and a vector velocity of (−167, 264, −95) km/s in a (ρ, ϕ, z) cylindrical coordinate system whose z axis is parallel to the rotation axis of the planet. At this time, the magnetic field (N. Ness, private communication, 1980) was within 3° of being entirely in a meridional plane, and in a meridional plane the field was oriented 37° below the equatorial plane pointing back toward Jupiter. The poloidal component of the above velocity is 30° below the equatorial plane and pointing back toward Jupiter. Hence there is an appreciable field-aligned component of the flow.

The spectra of Figure 13 are our clearest (and most pronounced) example of a general pattern of flow which is away from the equatorial current sheet on the dayside and toward it on the nightside. Figure 14 illustrates this pattern qualitatively for Voyager 1, and Figure 15 for Voyager 2. We plot the difference of the total flux density of positive ions into the B cup and the total flux density into the C cup, divided by the sum of these two flux densities. Since the B cup opens southward and the C cup opens northward, this difference will be positive if there is flow to the north and negative if there is flow to the south. The plots are linear against spacecraft event time. We indicate both radial distance from the planet and universal time at the top and local time at the bottom (1200 local time implies that the spacecraft lies in the plane that contains the Jupiter-sun line and is perpendicular to the Jovian orbital plane). In the figures we have also superimposed a graph of the spacecraft position perpendicular to the magnetic equatorial plane. Recall that passing through this plane essentially marks crossings of the Jovian current sheet, especially within 20 R_J of the planet. We note that the spectra in Figure 13 are from Voyager 2 inbound at ~1235 local time.

In the Voyager 1 curve we have not used data during a series of rolls for radio science just before and during occultation (1522–2002 UT on DOY 64) and during the outbound roll to Arcturus (0255–0320 UT on DOY 65). On Voyager 1 after 0255 UT on DOY 64 the plotted ratio is actually (A − B)/(A + B) instead of (B − C)/(B + C), as the roll to Arcturus reference fortuitously replaces the B cup with the A cup and the C cup with the B cup in spatial orientation. We also do not present data in the very cold region near closest approach on Voyager 1, since a significant part of the signal in the oblique B and C cups drops below the 10-V threshold of the instrument. The Voyager 2 data inbound begin just after the return of the spacecraft to Canopus orientation, after an approximately 11-hour interval off of Canopus. Otherwise, in these figures we plot data when fluxes in the oblique sensors are high enough to allow a significant comparison. Unfortunately, this limits us to fairly small distances from the planet (e.g., within ~25 R_J).

From these figures it is clear that in the dayside magnetosphere near noon, there is a marked tendency for plasma flow to be northward when the spacecraft is north of the magnetic dipole plane and southward when the spacecraft is south of that plane; i.e., the flow is away from the current sheet. The amplitude of the difference decreases to zero with decreasing radius and increasing local time toward dusk. In the dusk to midnight sector the difference again increases with increasing radius and increasing local time toward midnight. However, in this sector the plasma flow tends to be northward when the spacecraft is south of the magnetic equator, and vice versa; i.e., the flow is now toward the current sheet. Of course, this display gives us only information on the north/south flow and not on the radial component of flow. On Voyager 2 outbound near 1300 UT on DOY 191 the spacecraft is south of the current sheet, and the multisensor spectra are consistent with a poloidal velocity component which is northward and radially

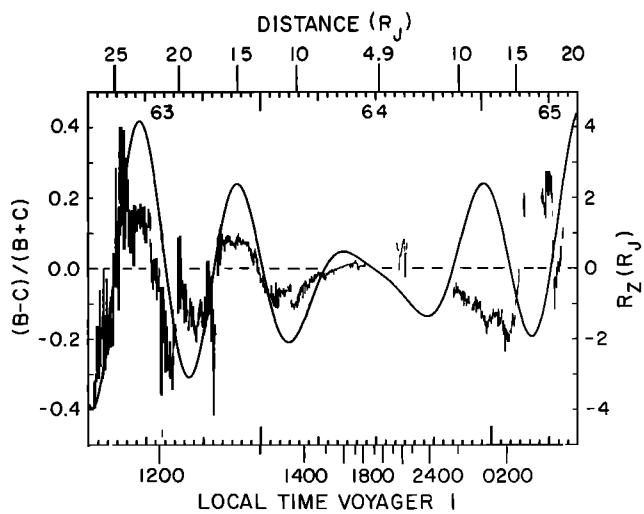

Fig. 14. A plot of the difference between the flux densities in the B and C cups divided by their sum for Voyager 1. We also show the vertical distance of the spacecraft from the magnetic equatorial plane. Local time is indicated at the bottom, and both distance from Jupiter and universal time are indicated at the top (DOY is given at 1200 UT).

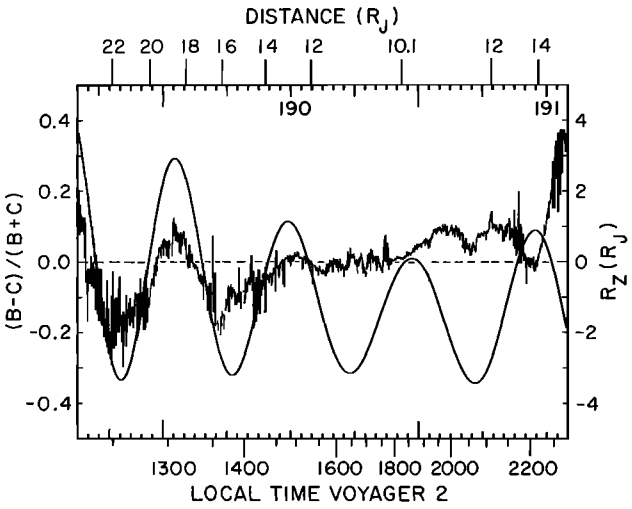

Fig. 15. A plot of the quantities shown in Figure 14 but for Voyager 2.

away from Jupiter. This nightside velocity is roughly consistent with field-aligned infall into the current sheet, as contrasted to outflow in the spectra in Figure 13.

Two further points should be made. First of all, as was noted above, the main sensor is oriented such that there would be slightly more purely azimuthal flow into the C cup than into the B cup on the inbound leg, and vice versa on the outbound leg. Even in the absence of any north/south flow we thus expect to see a negative signature in (B − C)/(B + C) inbound and a positive signature outbound. In fact, the differences in Figures 14 and 15 oscillate about a negative average value inbound and a positive average value outbound, as expected.

A more important point is whether the difference in the B and C fluxes is a unique signature of a north/south flow. If the plasma is isotropic in its rest frame, the answer is yes. If the plasma is highly anisotropic, one can think of scenarios where the answer is no. In particular, suppose the plasma is described by a bi-Maxwellian in which the thermal speed along the magnetic field is much greater than the thermal speed perpendicular to the magnetic field. On the dayside below the current sheet the C cup normal is closer to the magnetic field direction, and thus the C cup would sample a broader thermal distribution, with the B cup sampling a narrower distribution. On the dayside this difference convolved with the finite response of the detectors would produce a larger value of the C cup flux below the sheet, and vice versa above the sheet. On the nightside the reversal of the field orientation with respect to the PLS main sensor leads to the B cup normal being closer to the magnetic field direction below the current sheet, and thus the B cup would now sample a broader thermal distribution. On the nightside this difference convolved with the finite response of the detectors would produce a larger value of the B cup flux below the sheet and thus a reversal of the dayside pattern.

To investigate whether this scenario is responsible for the effect we interpret as north/south flow, we have used the simulation program described above and attempted to reproduce observed spectra (e.g., as in Figure 13) assuming purely azimuthal flow plus a large field-aligned thermal anisotropy. Although this model does, indeed, yield differences in the total fluxes in the B and C cups, it does not reproduce the spectral shapes in these cups, nor does it reproduce the relative flux levels observed in any three of the cups. In Figure 13, for example, a highly anisotropic plasma moving azimuthally will, in fact, have a C cup flux greater than the B cup flux, but the D cup flux in all such models is much greater than the C or B cup fluxes, contrary to observation. We conclude from a number of attempts of this sort that the observed difference in the B and C cup fluxes is, in fact, due to a north/south component of the plasma velocity. Quantitative estimates of the magnitude of these velocities on a global basis requires a much more complex least squares analysis of multisensor data, which is in progress. The one quantitative example we quote above in reference to Figure 13 should not be taken as typical, since it represents the most pronounced example of the phenomenon available. We note that these results are similar to those reported on the basis of anisotropies of MeV protons measured by the Pioneer spacecraft [*McDonald et al.*, 1979; *Northrop et al.*, 1979]. These authors report a field-aligned streaming of MeV protons away from the equatorial current sheet in the dayside middle magnetosphere. The trajectories of the Pioneer spacecraft were such that the nightside middle magnetosphere was not sampled appropriately for comparison with the Voyager data. Of course, there is no a priori reason that the field-aligned streaming of energetic particles and of thermal plasma should be coupled (whereas such reasons exist for motions perpendicular to the magnetic field).

Detailed Plasma Sheet Observations

We now turn from a discussion of global plasma properties to a detailed examination of the plasma sheet crossings. The plasma sheet is apparently a permanent feature of the Jovian magnetosphere. The fact that it undergoes large temporal variations on the dayside is demonstrated by the less regular structure displayed during Voyager 2 inbound as compared to the structure displayed during Voyager 1 inbound (cf. Figures 6 and 7). In addition, the sheet itself exhibits a great deal of fine scale structure in the characteristics of the plasma (cf. the spectral plot in Figure 25 in Appendix B covering the Voyager 1 current sheet crossing near 1400 UT on DOY 63).

The most regular variation in the plasma sheet was seen by Voyager 1 in the crossing near 1900 UT on DOY 63. Although the cooling effect is not as pronounced as it is during

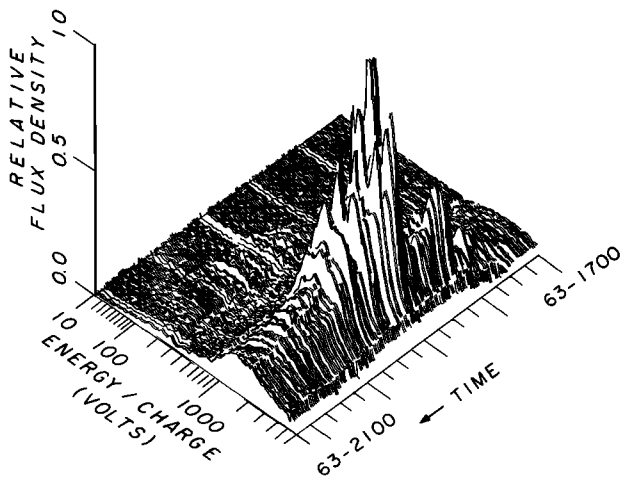

Fig. 16. A plot of the relative flux density of positive ion charge as measured in the D sensor (*M* mode) between 1700 and 2115 UT on DOY 63, 1979. The maximum value of the flux density in this time period is 4.5×10^6 proton charges per square centimeter per second.

other crossings (such as the one near 1400 UT on DOY 63), the spectra through this crossing show enough resolution in the L mode and M mode that we can analyze them in some detail. In Figure 16 we show the M mode spectra from 1700 to 2115 UT on DOY 63 as measured in the Voyager 1 side sensor. The format is the same as that used for Figure 25 in Appendix B. The heavy ionic species occupy the energy per charge scan from ~600 to ~4000 V. The increase in density and decrease in temperature which define the sheet crossing are readily apparent. The proton signal is lost in the noise in the M mode spectra but not in the L mode spectra. In Figure 17 we plot a representation of the L mode distribution function for the same time period. The presentation is the same as that used in Figure 26 in Appendix B and shows a well-defined proton signature for most of the time period concerned. The heavy ion peak signal is saturated in the L mode during most of this crossing and does not reflect the M mode variation. In order to analyze this crossing we fit the L mode spectra, using the M mode to fill in the saturated channels of the heavy ions. The parameters from the analysis are shown in Figure 18. The second panel from the bottom in Figure 18 shows the mass density in amu cm^{-3}. The density enhancement which delineates the sheet crossing shows that the plasma sheet is more or less centered on the current sheet crossing [*Ness et al.*, 1979*a*] at ~1915 UT as well as on the magnetic equatorial plane. The plasma sheet is about ~2 R_J thick and shows three smaller density enhancements, the largest being at the center and clearly discernible in Figure 18. The third panel shows the ratio of the total mass density to that of the protons. From this plot it can be seen that the first two internal density increases result from large enhancements in the heavy ions relative to the protons. It should also be noted that these places are precisely where the velocity component most nearly approaches the rigid corotation value, as shown in the fourth panel. The results are characteristic of the other plasma sheet crossings made by Voyager 1. The temperature of the protons from the L mode spectra analysis and of the (presumed) O^+ from the M mode analysis are shown in the top panel of Figure 18 along with the core electron temperatures [*Scudder et al.*, this issue]. *Scudder et al.* [this issue] discuss in detail variations in electron parameters through this crossing. Local cooling of the ions occurs at the larger mass

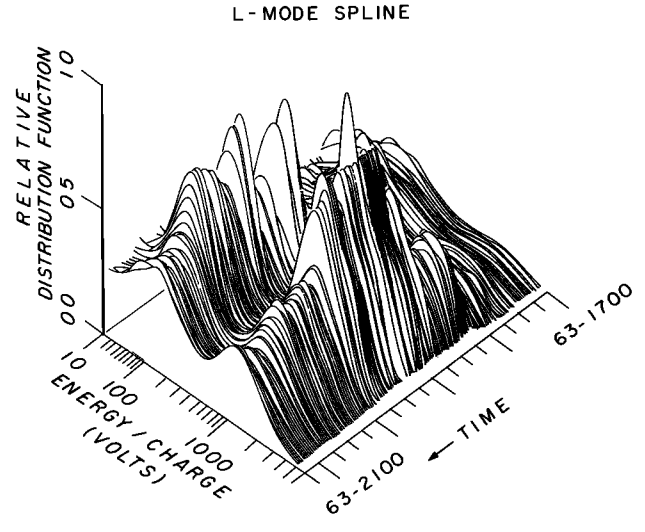

Fig. 17. A plot of the measured distribution function as measured in the D sensor (L mode) between 1700 and 2115 UT on DOY 63, 1979.

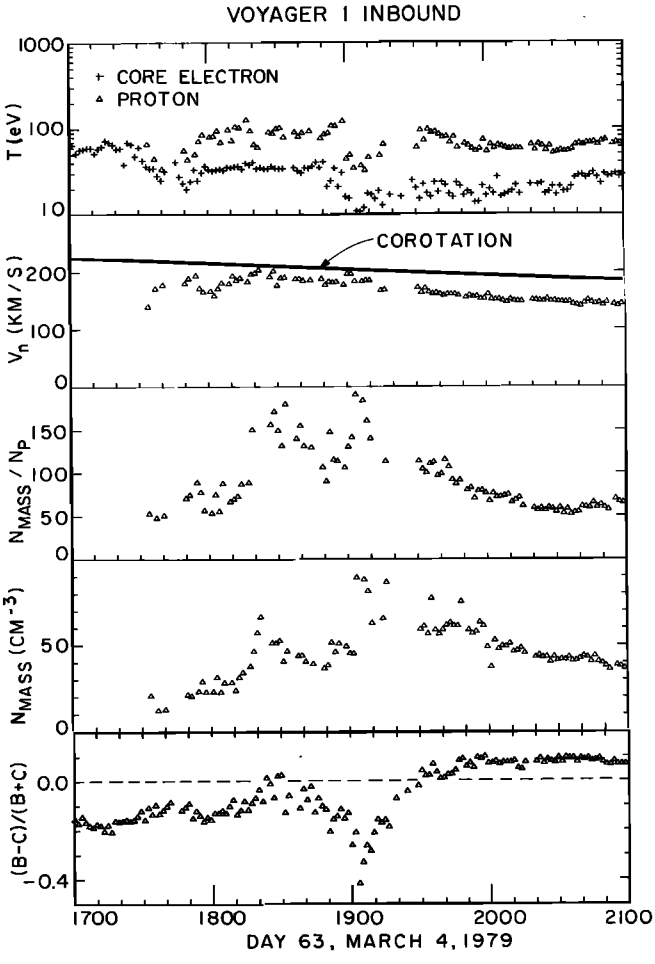

Fig. 18. A plot of plasma parameters for the plasma sheet crossing near 1900 UT on DOY 63, 1979.

density enhancements, although not to the same extent as has been observed in some of the other Voyager 1 crossings. To obtain an idea of the north/south flow pattern during this crossing, we plot in the bottom panel of Figure 18 the ratio of the difference of the flux densities measured in the B cup and C cup to their sum, as above. The maximum flux difference coincides with the maximum density and indicates that the plasma before ~1930 UT is moving southward and the plasma after ~1930 UT is moving northward.

At the center of this plasma sheet (~1900 UT), $\frac{1}{2}\rho V_n^2$ exceeds the magnetic energy density [*Ness et al.*, 1979*a*; see also *Scudder et al.*, this issue] by about a factor of 3 (i.e., the flow has become super-Alfvénic). This excess is facilitated by both the increased mass density in the plasma sheet and the decreased magnetic field strength in the current sheet. Away from the sheet, where the mass density is lower and the magnetic field strength higher, the flow is sub-Alfvénic. As we move outward on the dayside in the Voyager 1 encounter, every subsequent crossing shows this transition from sub-Alfvénic to super-Alfvénic flow. As we move inward from this crossing, the flow is invariably sub-Alfvénic. Interestingly enough, on Voyager 2 the crossings for which we have mass density estimates do not tend to show super-Alfvénic velocities. We attribute this difference from the Voyager 1 results to lower azimuthal velocities (see below) and to the lack of large mass density enhancements in the plasma sheet between ~12 and ~25 R_J.

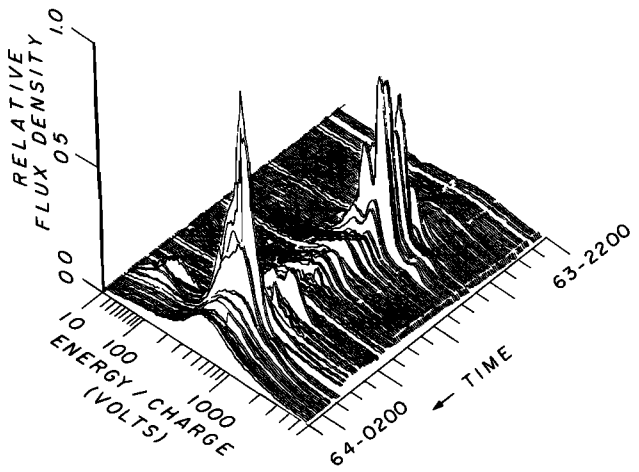

Fig. 19. A plot of the relative flux density as measured in the D sensor (*M* mode) between 2200 UT on DOY 63 and 0215 UT on DOY 64, 1979. The maximum value is 1.1×10^7 proton charges per square centimeter per second.

It is also important to note that NkT for the positive ions is usually a small fraction of $B^2/8\pi$ throughout this crossing and other crossings. For some of the cold, high-density *M* mode spectra the value of beta is as low as 1%. Although this is probably a lower limit, more typical values do not run more than 10–20%. Among other things this implies that the thermal pressure gradient of ions in the PLS energy range is negligible in terms of pressure balance across the current sheet. The electron pressures reported by *Scudder et al.* [this issue] are also not sufficient to balance the decrease in magnetic energy density. If the plasma sheet is in quasi-static equilibrium, pressure balance must be due to ions with energies above the Plasma Science energy per charge range of 6 kV. This conclusion is consistent with the results of *Krimigis et al.* [this issue].

Having considered one plasma sheet crossing quantitatively, we now consider qualitative properties of other crossings. Our distinction between plasma sheet and current sheet is most prominently exhibited in the Voyager 1 data around the beginning of DOY 64. The *M* mode spectra from 2200 UT on DOY 63 to 0215 UT on DOY 64 are shown in Figure 19. Only one current sheet crossing occurs during the time shown, and that at about 0000 UT on DOY 64 [*Ness et al.*, 1979*a*], between the two plasma sheet crossings. By itself, each plasma sheet signature is fairly typical and marked by increased density and decreased temperature. Relative differences include resolved peaks at mass to charge 32 (~2000 V) in the first crossing and resolved protons in the second crossing (~50 V at the center of the proton signature). In any quasi-static model of the plasma sheet it is hard to understand how mass density peaks can lie both north and south of the current sheet. However, the bifurcation of the sheet is more comprehensible if dynamic motion of the plasma is allowed. Again, flow out of the current sheet is indicated (cf. Figure 14). The plasma in the first density enhancement near 2315 UT on DOY 63 lies north of the sheet and appears to be moving northward, while that in the second enhancement at 0130 UT on DOY 64 lies to the south and appears to be moving southward. Hence plasma in the 'plasma sheet' may be in a dynamic state of motion relative to the current sheet, and the concept of a quasi-static magnetodisc may not be strictly correct. We discuss this point in more detail below.

As we have remarked, the dayside crossings of the plasma sheet inside of ~25 R_J by Voyager 2 were, in general, less regular than the crossings by Voyager 1 detailed above. The only two well-defined crossings inside of ~15 R_J occurred close to perijove, on DOY 190 near 2100 UT and on DOY 191 near 0930 UT. Figure 20 is a flux density plot of A cup spectra from 1800 to 2215 UT on DOY 190, which includes those spectra exhibiting the maximum density attained during the Voyager 2 encounter (cf. Figure 7). The cold spectral peaks occur at the approximate locations expected of corotating S^{3+} and S^{2+} or O^+, although they are highly time aliased. Note from Figure 7 that the maximum in density occurs below the magnetic dipole equator. The spectra associated with the crossing near 0930 UT on DOY 191 are similar to those in Figure 20 but are not as pronounced. The electron parameters in this later crossing are discussed by *Scudder et al.* [this issue].

DISCUSSION

The Azimuthal Velocity Component

A basic result of this study is the observation that the plasma in the middle magnetosphere on the dayside is not locked into rigid corotation with the planet. This lack of corotation had previously been suggested by the energetic particle anisotropies observed by Pioneer [*McDonald et al.*, 1979]. Most previous theoretical treatments had assumed either rigid corotation throughout the magnetosphere or a sudden change to a radially outflowing planetary wind at some distance from the planet. *Kennel and Coroniti* [1975] did question whether corotation could be enforced, but they discussed the issue in a somewhat different context.

Independent of the observation that the plasma in the middle magnetosphere is not rigidly corotating with Jupiter [*McNutt et al.*, 1979; *Kaiser and Desch*, 1980], *Hill* [1979] hypothesized that such an effect might be seen. His reasoning was that if the injection of plasma into the magnetosphere occurs rapidly enough and if the ionospheric (Pedersen) conductivity is low enough, a torque sufficient to enforce corotation cannot be transferred to the plasma as it moves outward. Hill derived the angular speed of the plasma as a function of cylindrical distance from Jupiter assuming cross-field transport in a dipolar magnetic field.

The Hill model is characterized by one parameter L_0, which

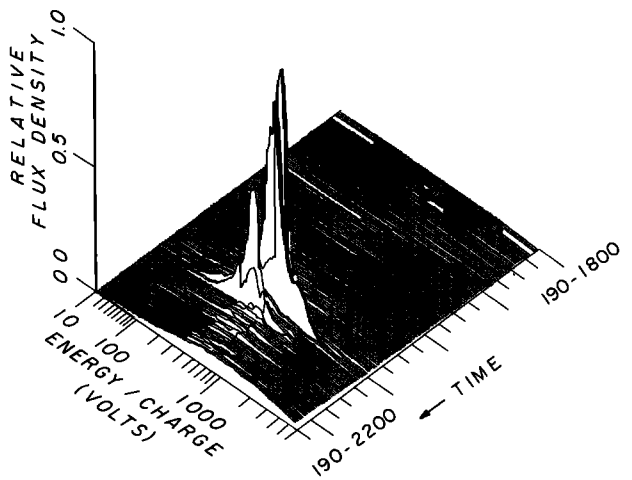

Fig. 20. A plot of the relative flux density as measured in the A sensor (*M* mode) between 1800 and 2215 UT on DOY 190, 1979. The maximum value is 7.5×10^7 proton charges per square centimeter per second.

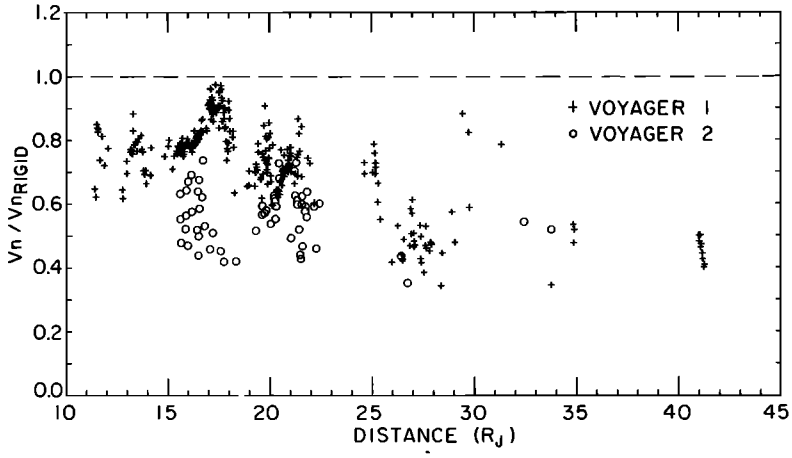

Fig. 21. A plot of the observed component of velocity into the D sensor divided by the component expected for rigid corotation for Voyager 1 and 2.

is the scale length for deviation from rigid corotation expressed in units of Jovian radii. If B_0 is the surface equatorial magnetic field, then in cgs units,

$$L_0^4 = \frac{\pi B_0^2 R_J^2}{c^2} \frac{\Sigma_p}{\dot{M}}$$

where $\dot{M}$ is the mass loading rate at the Io torus, Σ_p is the ionospheric height-integrated Pedersen conductivity, and c is the speed of light. Hence knowledge of two of the three quantities L_0, M, and Σ_p allows the third to be calculated. On the basis of the curve of *McNutt et al.* [1979], which is in agreement with the results presented here, *Hill* [1980] estimates L_0 to be 20 R_J. With a value for Σ_p of 0.1 mho, this value of L_0 implies $\dot{M} = 1 \times 10^{30}$ amu/s. This is in reasonable agreement with other estimates of $\dot{M}$ [*Broadfoot et al.*, 1979].

To first order, the bulk plasma motion is azimuthal on the dayside. In Figure 21 we plot as a function of radial distance the ratio of the observed velocity component into the side sensor to that which would be measured as a result of rigid corotation. Assuming that all of the bulk motion of the plasma is azimuthal (which is true to first order), this gives the ratio of the local to planetary angular velocity, which (according to Hill) is related to the height-integrated Pedersen conductivity Σ_p in the Jovian ionosphere and the mass injection rate $\dot{M}$ of the plasma into the magnetosphere.

The plots of normalized plasma angular velocity show three main features. First, at the same radial distance the magnetospheric plasma was rotating more slowly through the dayside during the Voyager 2 passage than during the Voyager 1 passage. In the context of the inertial loading model this implies a smaller height-integrated ionospheric conductivity Σ_p, a larger mass injection rate $\dot{M}$, or a less distended magnetic field configuration on the dayside. Second, there are indications of local maxima at the plasma sheet crossings. This may be a consequence of Ferraro's isorotation law [*Ferraro*, 1937]. If inertial loading is the cause of lack of corotation, then by Ferraro's theorem the angular velocity of the plasma should still be a constant along any given field line in the magnetosphere. The larger the L parameter the more torque required for corotation and hence the less the angular velocity. The largest local angular velocity should therefore be that seen during the current sheet crossing. The increase in angular velocity is most apparent in the Voyager 1 data in the combined crossings of both plasma and current sheets at 17 R_J (see also Figure 18). In the other crossings there is more scatter in the data, and the effect is not as discernible. Finally, the fractional angular velocity falls off roughly as r^{-1} (i.e., the azimuthal velocity component asymptotically goes to a constant) outside of 17 R_J in the Voyager 1 data. The case is less clear in the Voyager 2 data, although there is again some indication of a decrease with radial distance from Jupiter. Hill predicts an r^{-2} decrease in angular velocity, since at asymptotically large distances the field can no longer accelerate the plasma and the plasma conserves angular momentum as it moves outward.

Plasma Transport

If the decrease of angular speed with distance from Jupiter is an inertial loading effect, then plasma and angular momentum must be continually transported out of the Jovian magnetosphere. Conceivably, the transport could be convective (e.g., due to a continuous centrifugally driven wind), or the transport could be diffusive (e.g., due to flux tube interchange). There is no evidence for a centrifugally driven plasma wind either on the dayside or within 15 R_J of the planet on the nightside. We have already remarked that the principal component of plasma flow in the dayside magnetosphere is azimuthal. There are also radial and north/south flows superimposed on this azimuthal pattern, but these velocity components apparently are zero when averaged over local time (see below) and thus provide no net transport. In addition, Pioneer and Voyager magnetic field measurements in the middle magnetosphere [*Smith et al.*, 1974, 1975; *Ness et al.*, 1979*a*, *b*] have always shown a closed magnetic topology across the current sheet. This rules out a Weber-Davis convective outflow, such as *Kennel and Coroniti* [1975] had suggested for Jupiter. On the basis of these considerations we feel that a centrifugally driven wind in Jupiter's middle magnetosphere can be ruled out as a transport mechanism.

It is also conceivable that transport could occur due to aperiodic convection, as in the balloon mode instability [*Hasegawa*, 1979]. The approximate criterion for marginal stability in the balloon mode is obtained by setting the kinetic energy density of the plasma equal to the local magnetic field energy density. *Kennel and Coroniti* [1975] have suggested that attaining such marginal stability will lead to an opening of the field line topology, although *Goertz* [1976] has argued to the contrary. In those cases on Voyager 1 in which the current sheet and plasma sheet coincide, the Alfvénic Mach number ex-

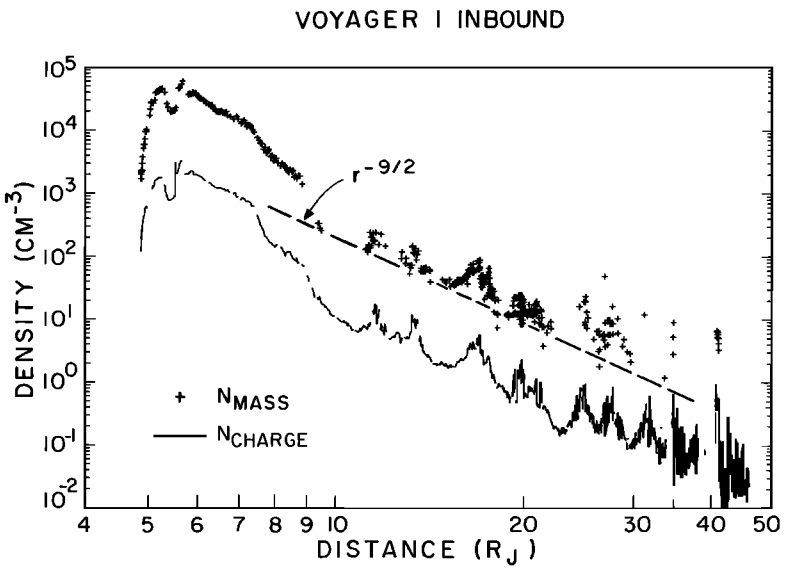

Fig. 22. A plot of the Voyager 1 densities versus distance.

ceeds unity without any drastic change in flow direction or plasma parameters, in accord with the theoretical conclusions of *Goertz* [1979]. Away from the sheets the magnetic field dominates the kinetic energy density of the plasma. On Voyager 2 the Alfvénic Mach numbers never exceed unity in those regions for which we have good estimates of the mass density. Available evidence thus indicates that the balloon mode instability is not operative in the middle magnetosphere and that there is no aperiodic convective plasma transport.

As transport is apparently not a result of either a steady or aperiodic 'wind,' it must be diffusive [*Siscoe,* 1977; *Goertz,* 1979]. Regardless of the diffusion mechanism, we can estimate an effective diffusion 'velocity' from the continuity equation and the assumption of azimuthal symmetry. Using Hill's best estimate of the injection rate, we can estimate the transport in the plasma sheet at, for example, the crossing at 1900 UT on DOY 63 for Voyager 1. Let the plasma sheet thickness be denoted by T, the L shell parameter by L, and the mass density by ρ. Then from continuity the outward transport velocity V_t is given by

$$\dot{M} = 2\pi R_J L T \rho V_t$$

Using values of $T = 2\ R_J$, $L = 17$, $\rho = 70$ amu cm^{-3}, and $\dot{M} = 10^{30}$ amu s^{-1}, we obtain $V_t = 13$ km/s. This value is consistent with primarily azimuthal flow, and thus the assumption of diffusive transport is not unreasonable.

We expect the radial profile of the mass density in the dayside magnetosphere to reflect the properties of the transport mechanism responsible for the diffusion of plasma outward from the Io torus. The most likely mechanism for transport is flux tube interchange diffusion driven by the centrifugal force on the azimuthally moving plasma. *Ioannidis and Brice* [1971] argued that corotation could perhaps be enforced even if interchange motions did occur. Conversely, the observation of lack of corotation argues that interchange motions will occur, if energetically favored, inasmuch as the same ionospheric conductance which topologically allows breakdown of corotation will also permit interchange motions. Such motions will drive the radial density gradient to a value consistent with marginal stability against the motion. Furthermore, once they are topologically allowed, interchange motions should limit the density well before the centrifugal instability becomes operable [*Ioannidis and Brice,* 1971; *Mendis and Axford,* 1974]. This should be true even in the presence of the current sheet [*Piddington and Drake,* 1968].

It can be shown that a full flux tube near the planet, surrounded by vacuum and initially corotating with the planet, will move outward by interchange with empty ones, and in doing so, exhibit an angular speed about the planet in accordance with *Hill*'s [1979] result. However, at some distance L_0 the outward velocity would equal the azimuthal velocity and then exceed that velocity at even greater distances. As we have noted, full flux tubes never interchange with toally empty ones, so this line of reasoning gives an upper limit to the outward transport velocity (the same type of calculation, assuming rigid corotation, was performed by *Mendis and Axford* [1974]). On the scale of the magnetosphere the process must be diffusive (via convection cells on a small scale [*Siscoe and Summers,* this issue]), resulting in a configuration of the plasma density which satisfies a marginal stability criterion.

Criteria for marginal stability for centrifugally driven interchange motions have been introduced by *Melrose* [1967] and *Hill* [1976]. Assuming a collisionless plasma counterstreaming along dipolar field lines from an ionospheric source, Hill finds that marginal stability is given by a density distribution in the equatorial plane which falls off as $r^{-9/2}$. A similar result with a slightly different behavior of the density holds if pressure gradients drive the instability [*Gold,* 1959].

For comparison, in Figure 22 we have plotted the mass density from Voyager 1 on a logarithmic distance scale. The profile is reasonably approximated by an $r^{-9/2}$ falloff outside of the torus region. This at least suggests that centrifugally driven flux tube interchange determines the density distribution. It should be noted that although Hill derived his result assuming an ionospheric source of plasma, the result should be applicable as long as there is a field-aligned streaming velocity component which increases linearly with distance from the planet. There is a flow velocity component along the field lines (see below), but the flow velocity dependence is not currently known. Perhaps more importantly in terms of interpretation of observations, the marginal stability criterion needs to be rederived, taking into account the field distortions

which result from a current sheet. We have also plotted the Voyager 2 density profile in this format [*McNutt*, 1980]. The results are again suggestive of a density profile determined by interchange diffusion.

The Plasma Sheet

On the basis of the Voyager 1 and Voyager 2 encounters, the Jovian plasma sheet is a permanent feature of the middle magnetosphere. However, the sheet obviously undergoes large temporal variations as evidenced by comparison of the Voyager 1 and Voyager 2 data sets (see Figures 6 and 7). The sheet is characterized by enhanced plasma density overall and a relative enhancement of heavy ions with respect to protons. In addition, the sheet (at least on the dayside) is relatively cool; i.e., the enhancement of heavy ions relative to that of the protons is associated with a cooling of all species. This is true of crossings of the sheet by both Voyager 1 and Voyager 2 and can be qualitatively verified from consideration of individual spectra even when quantitative analysis is not available. Comparing crossings of the sheet, there is also a tendency for the more abrupt crossings to exhibit lower temperatures. For example, in the Voyager 1 data the crossing at 1930 UT on DOY 63 shows a more spatially extended density increase than the other crossings. In the Voyager 2 data the crossings at 2100 UT on DOY 190 (Figure 20) and at 0930 UT on DOY 191 exhibit very localized structure and very cold spectra. The fact that cold ions and electrons are located in the plasma sheet crossings is a result that was unanticipated before the Voyager encounters. A qualitative explanation for this association is given by *Scudder et al.* [this issue].

The observed flows away from the equatorial current sheet on the dayside and toward it on the nightside are also unexpected. The local time asymmetry of the effect suggests an MHD pumping mechanism associated with the compression of the dayside magnetosphere by the solar wind. Without such compression, and in a steady state, the low-energy plasma would distribute itself along a given flux tube so as to balance the pressure gradient against the component of centrifugal force along the field lines. The scale height H for such a distribution is

$$H = \xi C_s/\omega$$

where C_s is the sound speed, ω is the angular speed of the plasma, and ξ is a dimensionless factor of order unity [*Hill and Michel*, 1976]. This equilibrium density distribution will be attained within a time scale of order H/C_s, or ω^{-1}. However, the plasma sheet is perturbed on this time scale by the dayside compression of the magnetosphere due to the solar wind. In principle, the plasma will never reach quasi-static equilibrium, and the continual imbalance of centrifugal and pressure gradient forces will give rise to a continuous acceleration of the flow away from and toward the magnetic equator.

Although the plasma in each flux tube is in continuous motion, the flow is such that the plasma sheet itself can exhibit a time stationary structure. To see this, we must follow a flux tube in its motion around the planet. As a given flux tube moves from midnight to noon, it will go from a maximally expanded to a maximally compressed configuration. The field constrains the plasma motion in the perpendicular direction, and the compression will be less at higher magnetic latitudes, closer to the planet. Hence the plasma will be accelerated along the field lines and eventually move to higher latitudes, in much the same way as toothpaste rushes out of a squeezed tube. In addition, the component of centrifugal force which confines the plasma to the equatorial plane will continually decrease as the flux tube moves from a stretched configuration far from the planet at midnight to a compressed configuration close to the planet at noon. The combination of these two effects will lead to a continual acceleration of the plasma away from the equatorial plane as the flux tube moves from midnight to noon; however, the flow velocity along the tube and this acceleration are not in phase. For a given flux tube the rate of compression will decrease to zero as the tube moves from dawn to noon, and the acceleration of plasma in the flux tube should correspondingly decrease to zero as the velocity along the field increases. At noon the flux tube will begin to expand, with a corresponding deceleration of the plasma, which will have achieved its maximum speed along the flux tube. At dusk the continuing expansion of the flux tube will have slowed the high-latitude plasma to zero velocity, when it is at its maximum latitudinal extent. As the flux tube moves past local dusk toward midnight, the plasma will begin to fall back toward the magnetic equator, achieving the largest infall velocity at local midnight, where the flux tube, at its greatest expansion, begins to contract again. Near dawn the plasma will have achieved its minimum latitudinal extent with zero velocity, as the contracting flux tube reverses the plasma infall to produce outflow once again. Since this process is cyclic, it involves no net plasma transport from the system. Thus we envision a plasma sheet which is dynamically expanding and contracting. The plasma is accelerated from midnight to noon and decelerated from noon to midnight, with the corresponding velocity away from the equator on the dayside and toward the equator on the nightside. The sheet is therefore thinnest near dawn and thickest near dusk in this simplified model. Such local time asymmetries will tend to increase in amplitude with increasing distance from the planet.

A sketch of this suggested global configuration is shown in Figure 23. We have included in the sketch the possibility of a north/south bifurcation of the plasma sheet. A simple linear analysis of the dynamics suggests that such bifurcation may arise naturally in this model. This would provide an explanation for the bifurcated plasma sheet crossings on Voyager 1, most notably on DOY 64 near 0000 UT (Figure 19) but also on DOY 63 near 1500 UT (Figure 25 in Appendix B).

We note that this picture is very different from what would be expected from a quasi-static expansion and contraction of the plasma sheet due to the solar wind interaction. A quasi-static process would produce a sheet which was thickest at

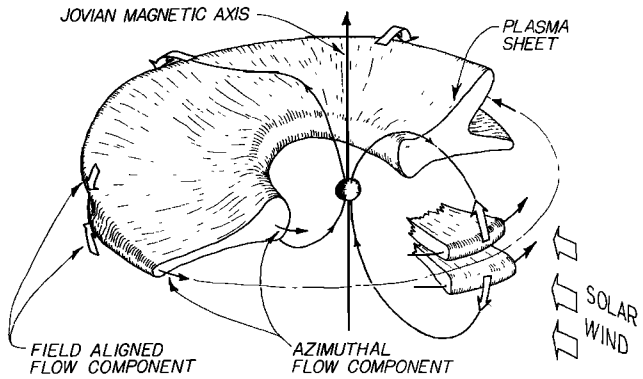

Fig. 23. A schematic of the dynamic plasma sheet model discussed in the text.

maximum compression (i.e., noon) and thinnest at minimum compression (i.e., midnight). Any small velocities associated with such a quasi-static process would be zero at noon and midnight and maximal at dawn and dusk. In contrast, the dynamical velocity pattern described above, especially its phase, arises only in the absence of quasi-static equilibrium. The possibility of such a pattern depends on the fact that the solar wind interaction tends to perturb a given flux tube on the same time scale as it takes the plasma to come to static equilibrium.

This picture of a dynamic plasma sheet is, of course, a gross oversimplification. In reality, even the most idealized model of such flow is nonlinear, and the actual interaction between plasma parcels accelerated in this fashion is complex. For example, the outflow velocity obtained from the spectra in Figure 13 is transonic for the protons and probably supersonic for the heavy ions, if they are at the same temperature as H^+. A similar supersonic infall on the nightside could lead to (for example) internal shocks. Admittedly, the spectrum in Figure 13 was picked precisely because it exhibited a large nonazimuthal velocity component, and thus the flow here is not typical. However, the example makes apparent the problems in any realistic treatment of the flow. Even so, on the basis of simple physical arguments we are reasonably confident that a proper treatment will produce a velocity pattern whose phase with respect to local time is roughly in accord with our simple model above and thus in accord with the observed phase displayed in Figures 14 and 15.

A more serious objection to this model is the question of whether the solar wind interaction can actually produce such effects as deep in the magnetosphere as is indicated in these figures. In part, the answer to such objections lies in theoretical studies of the stability of the magnetodisc to lateral perturbations. In part, the answer also lies in a more complete observational study of the magnitude of this velocity effect as a function of radial distance. Such a study is in progress (S. Olbert, personal communication, 1980).

There is one further dynamical aspect of this hypothesized plasma sheet configuration which is of note. Since the poloidal flow is principally field aligned and the field lines are appreciably curved in the vicinity of the magnetic equator [*Connerney et al.*, this issue], there exists along the sheet an inertial force perpendicular to the magnetic field in a meridional plane. In general, regardless of the direction of the flow, this results in a component of centrifugal force which is perpendicular to the magnetic equatorial plane and which acts on the field lines so as to distend them away from that plane, thus increasing the thickness of the current sheet. Hence magnetic tension perpendicular to the magnetic equator is balanced by an inertial force as well as by a pressure gradient force. Therefore a description of the vertical momentum balance in the sheet based on pressure balance alone is, in principle, insufficient, and estimates of the sheet temperature based on pressure balance alone will be overestimates. In practice, the importance of such an effect remains to be evaluated.

In summary, it is clear that the Jovian plasma sheet is a complex structure. In the middle magnetosphere the sheet diffuses plasma and angular momentum outward rapidly enough that the magnetic field lines threading it slip with respect to Jupiter. At energies per charge below 6 kV the ions in the sheet are cold and dense, with sufficient streaming energy to significantly influence the magnetic field topology of the sheet but with essentially negligible thermal energies. Flows away from and toward the equatorial current sheet suggest that the plasma sheet is an inherently time-dependent structure which is not in quasi-static equilibrium [*Belcher and McNutt*, 1980]. An accurate assessment of the magnitude of departures from equilibrium requires a complete analysis of vector velocities of the magnetospheric plasma. Such a study is beyond the scope of this work.

Overall, the Jovian magnetosphere has proven to be neither earthlike nor pulsarlike. It is instead a unique plasma construct in many ways, apparently as a result of the venting of heavy ions from the Jovian moon Io. This uniqueness alone makes the Jovian magnetosphere worthy of further scientific inquiry. In addition, its presence in the solar system allows us the opportunity of making in situ observations of plasma confined by a fast magnetic rotator, a subject of general physical and astrophysical interest.

APPENDIX A: POSITIVE ION SPECTRAL ANALYSIS—METHOD

We consider in detail the information that can be obtained from quantitative analysis of D cup spectra. The Faraday cup is an electrostatic device which measures positive ion properties as a function of energy per charge. The measured electric currents are related to the positive ion distribution function in the following way [*Vasyliunas*, 1971; *Belcher et al.*, 1980]. Consider the response of the cup to an ionic species of mass number A, charge number Z^*, and distribution function $f(\mathbf{v})$. Let the set of contiguous potentials which define the energy per charge channels be $\{\phi_j\}_{j=1}^{K+1}$, where K is 16 (L mode) or 128 (M mode). This defines a corresponding set of particle velocities $\{v_j\}_{j=1}^{K+1}$, where

$$v_j = (2eZ^*\phi_j/Am_p)^{1/2} \tag{1}$$

with e and m_p being the proton charge and mass, respectively. In the jth channel the measured current is due to particles with an average velocity component of

$$\bar{v}_j = (v_{j+1} + v_j)/2 \tag{2}$$

in a velocity window of width

$$\Delta v_j = v_{j+1} - v_j \tag{3}$$

Given the effective area of the cup at normal incidence (including transparency), A_{eff}, and the response function of the instrument, $G_j(\mathbf{v}, \hat{\mathbf{n}})$, the current I_j measured in the jth channel is

$$I_j = eZ^*A_{\text{eff}} \int_{v_j}^{v_{j+1}} v_n \int_{-\infty}^{\infty} \int_{-\infty}^{\infty} f(\mathbf{v})G_j(\mathbf{v}, \hat{\mathbf{n}})\, dv_{t_1}\, dv_{t_2}\, dv_n \tag{4}$$

where the subscript n denotes the velocity component parallel to $\hat{\mathbf{n}}$ in velocity space and the subscripts t_1 and t_2 refer to the orthogonal components perpendicular to $\hat{\mathbf{n}}$.

In our analysis we assume that the distribution function is a convected, isotropic Maxwellian characterized by density N, thermal speed W, and bulk velocity V. Then

$$f(\mathbf{v}) = \frac{N}{W^3\pi^{3/2}} \exp\left[-\frac{(\mathbf{v}-\mathbf{V})^2}{W^2}\right] \tag{5}$$

The response function for the side sensor can be characterized by parameters α_j, of the order of unity [*Binsack*, 1966; *Sittler*, 1978; S. Olbert, private communication, 1980], as follows:

$$G_j(\mathbf{v}, \hat{\mathbf{n}}) = \exp\left[-\alpha_j v_t^2/v_n^2\right] \tag{6}$$

where $v_t^2 = v_{t_1}^2 + v_{t_2}^2$. The transverse integrations in (4) can be carried out analytically to yield

$$I_j = eZ^*A_{\text{eff}} \int_{v_j}^{v_{j+1}} v_n\, dv_n F(v_n) \frac{v_n^2}{v_n^2 + \alpha_j W^2} \exp\left[-\frac{\alpha_j V_t^2}{W^2\alpha_j + v_n^2}\right] \tag{7}$$

where

$$F(v_n) = \frac{N}{\pi^{1/2} W} \exp\left(-(v_n - V_n)^2/W^2\right) \tag{8}$$

is the reduced distribution function along the cup normal and the bulk flow components normal and transverse to the cup are V_n and V_t, respectively.

In principle, the measured currents are sensitive to both V_n and V_t. However, the influence of V_t on the currents is too slight to be observable unless $V_t > V_n$ (e.g., flow very oblique to the cup normal). In practice, we do not analyze flows which are highly oblique because our confidence in the validity of expression (6) for $G_j(\mathbf{v}, \hat{\mathbf{n}})$ is low for high angles of incidence. For the cases we consider herein, it is reasonable to assume that the bulk flow is within ~20° of the cup normal; thus V_t^2/V_n^2 is small, and the exponential in (7) can be approximated as unity for those values of v_n for which $F(v_n)$ gives an appreciable contribution to the integral. This will introduce errors of order V_t^2/V_n^2 in resulting estimates for N, V_n, and W. The errors introduced are such that estimates for V_n and W will be high and estimates for N low for Mach numbers greater than unity.

Equation (7) with V_t set to zero is thus our basic equation relating the observed currents to the model parameters N, W, and V_n. It is this relation that we use in our least squares fit procedure. The details of this procedure are described by *McNutt* [1980].

It is useful to consider (7) in the following limit. In many cases of interest, the ions are supersonic ($V_n \gg W$), but the thermal speed is still large in comparison with the width of the velocity windows in the M mode ($W \gg \Delta v_j$). With these two additional assumptions, (7) becomes

$$I_j = eZ^*A_{\text{eff}} \bar{v}_j \Delta v_j F(\bar{v}_j) \tag{9}$$

Using (1)–(3), we find that

$$\frac{I_j}{A_{\text{eff}} e^2(\phi_{j+1} - \phi_j) m_p} = \frac{(Z^*)^2}{A} F(\bar{v}_j) \tag{10}$$

All quantities on the left-hand side of (10) are known. Thus for a supersonic flow within ~20° of the D cup axis the currents I_j as measured in the high-resolution M mode can be directly related to the reduced distribution function via (10). If the flow is transonic (Mach numbers of order unity) or if we are dealing with low-resolution L mode data, (10) is very approximate, and we must return to the integral (7) to relate F and I_j properly. In any case, for data display (as, for example, in Figure 3) we plot the quantity shown on the left-hand side of (10). We loosely refer to this as the 'measured distribution function,' even though it actually gives the distribution function scaled by $(Z^*)^2/A$, and this only approximately so for the transonic case and/or L mode data. We also display positive ion data by plotting I_j/eA_{eff} versus energy per charge (as, for example, in Figure 5). This quantity is the charge flux density of positive ions, in units of proton charge per square centimeter per second.

The measured current in the jth channel is actually a sum of terms as in (4), each computed for a particular ionic species. In such a case a display of the left-hand side of (10) will yield a superposition of ionic distribution functions, each scaled by the appropriate value of $(Z^*)^2/A$. Furthermore, if a set of ionic species with mass and charge numbers $\{A_i, Z_i^*\}_{i=1}^N$ are moving into the cup with the same velocity component V_n and if all species are reasonably supersonic, then the measured distribution function will show a series of peaks at energies per charge of A_i/Z_i^* times the proton energy per charge. If we can identify the energy per charge of the proton peak, we can determine the mass to charge ratios of the ionic species producing peaks at higher energies per charge. Even if we do not know the energy per charge of protons, we can usually deduce the mass to charge ratios of the heavier ionic species, if two or more are present, by comparison of the various ratios of observed energy per charge. Knowing the mass to charge ratios, we can then deduce the common velocity.

From this discussion it is clear that we can only determine the ratio A_i/Z_i^* and not A_i and Z_i^* individually. For example, O^+ has the same mass to charge ratio as S^{2+} and will appear at the same energy per charge as S^{2+} in our measured spectra. This is a basic ambiguity in the measurement. We use various physical considerations to argue, for example, whether the 16 peak should be mostly O^+ or S^{2+} (see Appendix B). However, we emphasize that even though we may misidentify A_i or Z_i^* separately, as long as we correctly identify the ratio A_i/Z_i^* for a set of ionic species, we will obtain the correct total charge and mass density of the plasma. To show this, suppose we have obtained a set of densities and thermal speeds $\{N_i, W_i\}_{i=1}^N$ for species with mass to charge ratios $\{A_i/Z_i^*\}_{i=1}^N$ (which we take to be known from comparison of observed energies per charge). Then the total charge density N_+ in units of the proton charge is

$$N_+ = \sum_i Z_i^* N_i \tag{11}$$

and the total mass density N_M in units of the proton mass (ignoring the small correction due to the mass defect) is

$$N_M = \sum_i A_i N_i \tag{12}$$

From (8) and (10) it is clear that if we know A_i/Z_i^*, then $Z_i^*N_i/W_i$ is a measured quantity and thus independent of our individual choice of A_i and Z_i^*. But W_i is also independent of this choice, since particle velocities scale as $(A_i/Z_i^*)^{1/2}$ (see equation (1)). Thus $Z_i^*N_i$ is an invariant, as is A_iN_i, since A_i/Z_i^* is known. Even if we incorrectly identify A_i and Z_i^* separately, we always arrive at the correct total mass and total charge densities if we know the mass to charge ratio A_i/Z_i^*.

Thus far, we have been assuming that the various species have a high enough Mach number that the energy per charge peaks are well defined for different A_i/Z_i^*. It is easily seen that the peak in energy per charge of the ith species will be within a thermal width of the peak of the $(i + 1)$th species when

$$W_{i+1}/V_n \gtrsim 1 - (A_iZ_{i+1}^*/Z_i^*A_{i+1})^{1/2} \tag{13}$$

For A_i/Z_i^* values of 1 and 8, s trong overlap will occur only for Mach numbers $\lesssim 1$. However, for values of 8 and $10\frac{2}{3}$ or $10\frac{2}{3}$ and 16, strong overlap occurs for Mach numbers $\lesssim 6$. Thus we lose resolution in the heavy ions even at relatively high Mach numbers, and identification of individual A_i/Z_i^* peaks for the

TABLE 1. Ionization Potentials and Mass to Charge Ratios of Various Ions

	I	II	III	IV	V
H	13.6	··· (1)	···	···	···
He	24.6	54.4 (4)	··· (2)	···	···
O	13.6	35.1 (16)	54.9 (8)	77.4 (5⅓)	113.9 (4)
Na	5.1	47.3 (23)	71.6 (11½)	98.9 (7⅔)	138.4 (5¾)
S	10.4	23.3 (32)	34.8 (16)	47.3 (10⅔)	72.7 (8)
K	4.3	31.6 (39)	45.7 (19½)	60.9 (13)	82.7 (9¾)

Ionization potential values are in electron volts.

heavy ions becomes difficult. This happens in many of the observed spectra. Even here, however, it is easily seen from (7) that as long as all species are within our energy per charge range and reasonably supersonic, then

$$\sum_j I_j = eA_{\text{eff}}V_n \sum_i N_i Z_i^* \tag{14}$$

and thus

$$N_+ = \sum_j I_j/(eA_{\text{eff}}V_n) \tag{15}$$

Provided that we have an estimate of V_n from other sources, we can estimate N_+, even though the individual peaks cannot be identified.

APPENDIX B: POSITIVE ION SPECTRAL ANALYSIS—EXAMPLES

We first consider the best examples of our high-resolution positive ion spectra. Figure 3 is a plot of measured distribution function versus energy per charge for an *M* mode taken on DOY 63 at 1537:35.1, near 19.8 R_J. The spectrum shown is from a 20-min period in which the plasma density was high enough and temperatures low enough that the *M* mode flux is well above the noise level for most channels and all dominant species within the energy per charge scan of the instrument are resolved. We analyze this spectrum by utilizing a set of assumptions and then checking these for consistency. We assume that the plasma is multicomponent in nature, and we further assume that each component is well represented by a convected, isotropic Maxwellian distribution function. Since the convective velocity is expected to be almost antiparallel to the (outwardly directed) normal of the D sensor and the magnetic field is nearly perpendicular to the normal, we assume that the species have a common velocity component (i.e., they are 'comoving') into the sensor. In general, there could be field-aligned differential streaming among the components, but this should be a negligible effect for spectra measured with the D cup.

As there are ample sources of hydrogen in the Jupiter environment and the lowest mass to charge ratio is that for H^+, we assume that the peak at the lowest energy per charge in Figure 3 is due to H^+. Various ions of oxygen and sulfur have been identified in the Jovian magnetosphere. *Broadfoot et al.* [1979] report that the dominant emitting species in the Io torus are S^{2+}, S^{3+}, and O^{2+}. The Plasma Science instrument has observed species with mass to charge ratios of 1, 8, 10⅔, 16, 23, 32, and 64 [*Bridge et al., 1979a, b*; *Sullivan and Bagenal,* 1979]. *Sullivan and Bagenal* [1979] have noted that such ratios result from protons, oxygen, sulfur, sodium, and sulfur dioxide. Figure 3 shows some of these characteristic peaks.

As a guide to the interpretation of this spectrum, we list in Table 1 the ionization potentials of various ions which may be present in the Jovian magnetosphere. We also list the mass to charge ratios for the various ionization states. We can draw some qualitative conclusions about the probable ionization states present in this spectrum as follows. The peak at 8 could

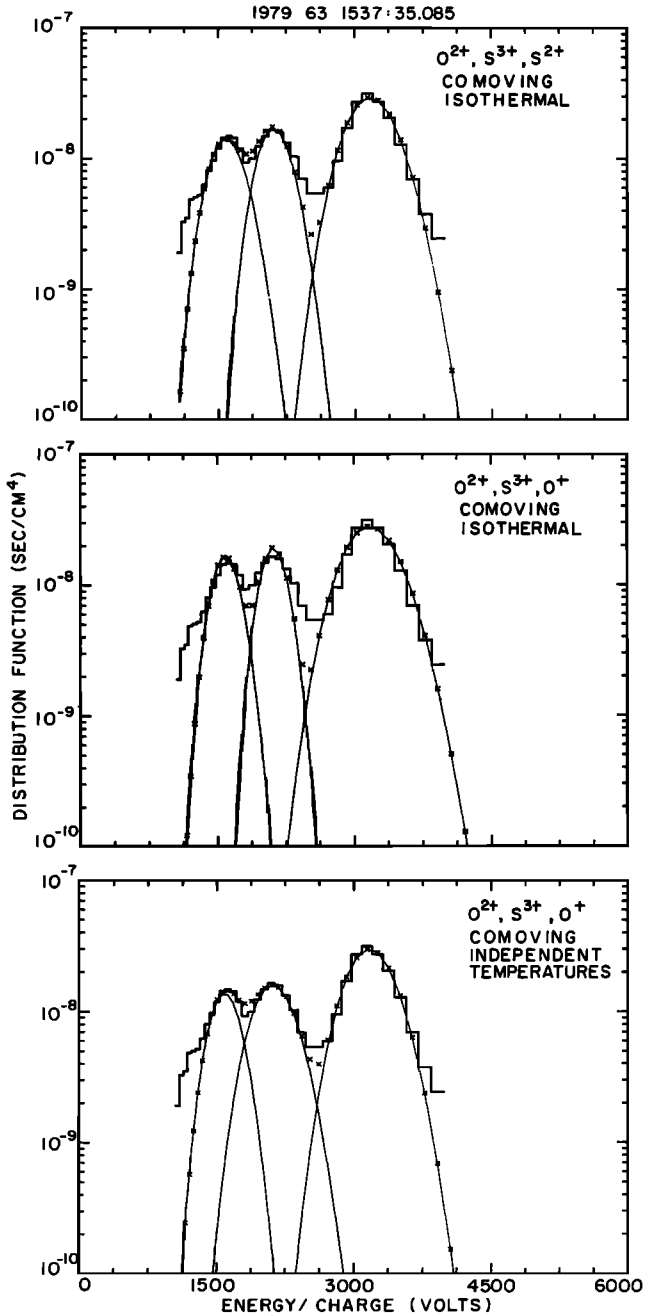

Fig. 24. Fits to the *M* mode spectrum shown in Figure 3. Only that part of the spectrum used in the fit is shown. The individual Maxwellians are shown by thin lines, and their summed contributions in each channel are shown by crosses.

be due either to O^{2+} or to S^{4+}. The presence of S^{4+} requires ionizing energies of 47 eV. However, there is no indication of the present of significant amounts of O^{3+} at $5\frac{1}{3}$, which requires ionizing energies of 55 eV. In addition, the peak at $10\frac{2}{3}$ is almost certainly S^{3+}, which requires ionizing energies of 35 eV. These considerations suggest that in its past, the observed plasma population was exposed to some ionization mechanism of at least 35 eV in characteristic energy but not as large as 55 eV. On this basis the peak at mass to charge of 8 is most likely O^{2+} and not S^{4+}, and we assume the former identification in the analysis of the data. The peak at 16 is more of a problem. Consideration of ionization energies and the fact that there is a significant amount of O^{2+} and S^{3+} would suggest that the signal is most probably due to sulfur, with most of the oxygen in the doubly ionized state. However, this is not necessarily true, as discussed in more detail by *Bagenal and Sullivan* [this issue] and *McNutt* [1980].

To put the analysis of this spectrum on a more quantitative basis, we have fit various parts of the spectrum in Figure 3 with eleven different sets of assumptions. These and other fits to resolved *M* mode spectra are discussed at length by *McNutt* [1980], and we report only the most pertinent results here. Since the peaks at 8, $10\frac{2}{3}$, and 16 are well defined and dominant, we first assume that this part of the spectrum is due to three comoving, isotropic Maxwellians, each with an independent temperature and density (a seven-parameter fit). We have assumed a composition of O^{2+}, S^{3+}, and O^{+}, although the 16 peak could as well be S^{2+} or (as is likely) a combination of O^{+} and S^{2+} with different thermal speeds. In the bottom panel of Figure 24 we show the fit currents. Only that part of the spectrum used in the fit is shown. The individual Maxwellians are shown by thin lines, and their summed contribution in each channel is shown by crosses. The common velocity is 195 km/s. The fit temperatures of O^{2+}, S^{3+}, and O^{+} are 16, 36, and 10 eV, respectively, with number densities of 0.14, 0.15, and 0.95 cm^{-3}. The value of the total charge density N_+ for these three species is 1.67 proton charges /cm^3, and the value of the mass density N_M is 22.2 amu/cm^3.

The ion temperature is probably the most ill-defined quantity in this fit, since it is dependent upon the complete definition of the peaks (i.e., is the peak at 16 due to O^{+} or S^{2+} or both). In the fit quoted above, a comparison of the various temperatures and temperatures per amu shows that both of these quantities vary from component to component. Assuming that the peak at 8 is all O^{2+} and the peak at $10\frac{2}{3}$ is all S^{3+}, it appears that the thermal speed, rather than the temperature, tends to be the same for each of these heavy ion components. This is consistent with ionization and pickup by the magnetic field of a collisionless plasma [*Bagenal and Sullivan*, this issue]. However, the thermal speed of the 16 peak is somewhat low.

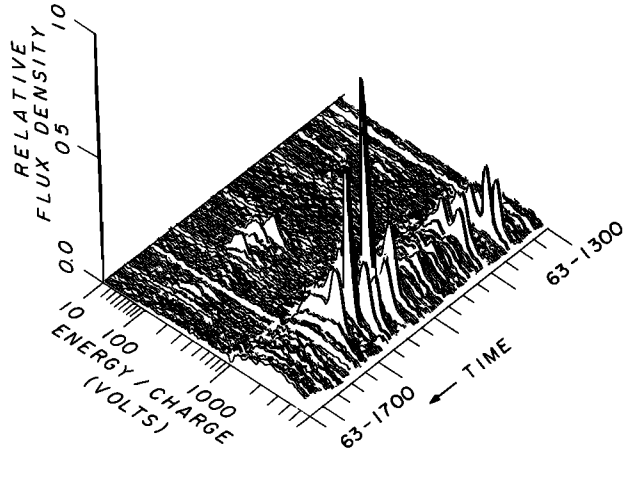

Fig. 25. A plot of the flux density of positive ion charge as measured in the D sensor (*M* mode) between 1300 and 1715 UT on DOY 63, 1979. The flux density has been normalized to the largest value seen in the entire time period. The maximum is 3.4×10^6 proton charges per square centimeter per second.

For comparison, we have also fit this portion of the spectrum assuming comoving O^{2+}, S^{3+}, and O^{+} at a common temperature (a five-parameter fit). The fit currents are shown in the middle panel of Figure 23. The common velocity is again 195 km/s, with a common temperature of 13.5 eV. The individual number densities are 0.15, 0.11, and 1.02 cm^{-3}, with values of N_+ and N_M of 1.65 cm^{-3} and 22.3 amu/cm^3.

We have also fit the spectrum assuming comoving O^{2+}, S^{3+}, and S^{2+} at a common temperature. The fit currents are shown in the top panel of Figure 23. The common velocity is 195 km/s, with a common temperature of 22.2 eV. The individual densities are 0.17, 0.12, and 0.49 cm^{-3}, with values of N_+ and N_M of 1.68 cm^{-3} and 22.2 amu/cm^3.

From these and other fits to the dominant ion peaks at 8, $10\frac{2}{3}$, and 16 we conclude that neither the assumption of common thermal speed nor that of common temperature is an accurate description of the heavy ions. Although the temperature estimates vary by factors of 2–3 from one case to another, it is important to note that the common velocity component and the values of N_+ and N_M for these ions are almost totally unaffected by the different assumptions, as we would expect from the discussion in Appendix A.

Ionic species with larger mass to charge ratios than 16 also contribute to the inertia of the plasma, notably Na^{+} at 23 and S^{+} at 32. Usually S^{+} is above our energy per charge range outside of $\sim 10\ R_J$, although it appears in a few *M* mode spectra (for example, the spectrum at 1550 UT on DOY 63, as shown in the works by *Sullivan and Bagenal* [1979] and *Belcher et al.* [1980]). Estimates of the densities of Na^{+} in the spectrum of Figure 3 and of S^{+} in the 1550 UT spectrum indicate that these species contribute at most 20% to the total inertia of the positive ions. We, of course, expect most of the sulfur to appear as S^{2+} and S^{3+}, in any case.

We have also fit an independent Maxwellian to the H^{+} peak in Figure 3, obtaining a number density of 0.19 cm^{-3} and a temperature of 9.4 eV. The H^{+} ions thus constitute less than 15% of the total charge density and less than 1% of the total mass density. The H^{+} thermal speed is far higher than that of the heavy ions, leading to an H^{+} temperature which is comparable to that of O^{+}. This is typical of those few spectra in which simultaneous but independent H^{+} and O^{+} fits to the *M* mode spectra are possible. The value of V_n for H^{+} from the fit is 183 km/s, significantly different from the 195 km/s exhibited by the heavy ions. This difference could be due to a positive spacecraft potential of the order of 20 V, as discussed in the main text. However, it could also be due to time aliasing, since variations in V_n of 20 km/s from one *M* mode spectrum to the next are not uncommon. It should be remembered that the spectrum in Figure 3 is a composite and that the measurements below 400 V, which define the H^{+} peak, are taken 96 s earlier than the measurements above 400 V, which define the heavy peaks. The time of the spectrum is associated with the measurements of the heavy peaks. For reference, we note that the value of N_+ obtained from the total flux density of this

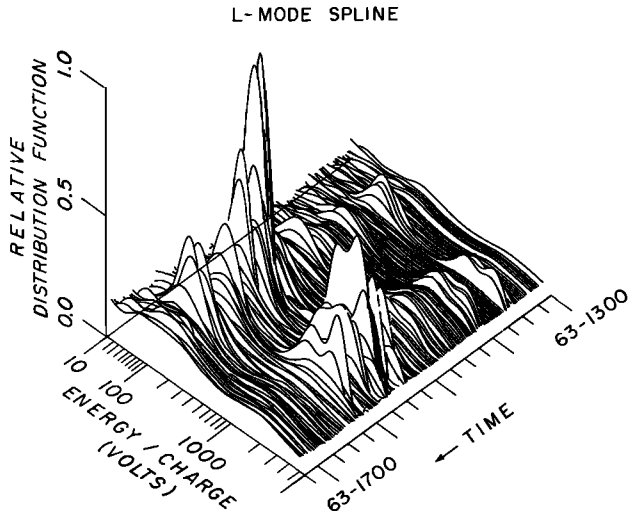

Fig. 26. A plot of the positive ion distribution function as measured in the D sensor (L mode) between 1300 and 1715 UT on DOY 63. The 16 L mode channels have been fit by a 128-channel spline for a clearer display of the data. The distribution function has been normalized to the largest value in the time period.

spectrum, as described above, is 2.0 cm^{-3}. The adjacent electron density obtained by *Scudder et al.* [this issue] at 1538 UT is 1.6 cm^{-3}.

In Figure 25 we show spectral data which include a plasma sheet crossing and the M mode spectra just discussed (1537 and 1550 UT on DOY 63). The figure shows a 4 hour and 15 min run of M mode spectra from 1300 to 1715 UT as measured in the D cup on Voyager 1 inbound. The spectra are plotted as flux density versus channel number. The flux density has been normalized to the largest value seen during the entire time period, and the channel number scale is linear and has been labeled with tick marks at the appropriate energy per charge values. It should be noted here that the flux density scale is linear, while the individual spectral plots are distribution functions plotted on a logarithmic scale. Also, a plot of distribution function tends to emphasize the H^+ compared to the heavy ions, while a plot of flux density tends to emphasize the heavy ions.

The figure gives a good representation of the variability of the data. The peak at 16 in the 1537 UT spectrum is the highest peak in the figure. While individual spectra show peaks which look well defined and Maxwellian, variations in all the fit parameters from spectrum to spectrum can be significant. In this time period, density increases associated with the plasma sheet can be seen centered around 1345 and 1550 UT, while the magnetic field minimum (indicative of the center of the current sheet) occurs at about 1400 UT [*Ness et al.*, 1979*a*]. The heavy ions occupy the energy per charge range of 1000–6000 V. The H^+ signals occur at about 100 V, and in the sequence shown, only three spectra show H^+ signals prominently above the noise level. This is a typical problem with the H^+ signal in the M mode data. It is readily apparent from Figure 25 that many of the M mode spectra are in the noise and cannot be fit. The situation is very different in the adjacent L mode spectra. Since the channel widths in energy per charge are a factor of 8 larger than those of the M mode, there is a gain in the signal-to-noise ratio, thus improving the H^+ signal. At the same time, the energy per charge resolution decreases, so that the plasma parameters for the ionic species other than H^+ are more uncertain. The situation is illustrated in Figure 26, where we show a spline fit representation for the L mode data in the same period as that shown in Figure 25. To emphasize the H^+ signal, we have plotted distribution function versus channel number, both on a linear scale.

In Figure 4 we have shown the L mode spectrum taken 1 min after the M mode spectrum of Figure 3. Here the lack of resolution of the heavy ions is apparent. The protons, however, remain as a resolved separate peak. Frequently, the L mode spectra show such a signature, even when the Mach number is low. In this example the fact that the 16 peak is separated from the others in the M mode is clearly reflected in the peak in the fourteenth channel of the L mode. In other cases where the M mode spectra are unresolved, the corresponding L mode data exhibit two smooth peaks, one from protons and the other from heavy ions.

The L mode spectra never contain enough information to allow an unambiguous fit to the heavy ion 'peak.' Even assuming the same velocity component for all species and the same temperature for the major contributors (O^{2+}, S^{3+}, and O^+ or S^{2+}), we are left with too many free parameters for the fitting procedure to produce reasonable results. By assuming only two heavy species, however, we can obtain useful information. For example, consider a series of fits to the L mode spectrum shown in Figure 4. This spectrum should yield plasma parameters close to those found in our detailed M mode analysis discussed above, although as Figures 25 and 26 show, there can be great variability on a time scale of 1 min. To limit the number of fit parameters, we have assumed a common bulk velocity component and a common temperature for the heavy ion species, with an independent temperature for H^+.

In the bottom panel of Figure 27 we show a fit assuming a composition of H^+, S^{3+}, and O^+. This fit yields a common speed of 184 km/s, an H^+ temperature of 12 eV, and a heavy ion temperature of 43 eV. The individual number densities are 0.23, 0.14, and 1.14, respectively, yielding a value of N_+ of 1.8 cm^{-3} and a value of N_M of 23.1 amu/cm^3. In the center panel we show a fit assuming a composition of H^+, O^{2+}, and S^{2+}. The common speed is 183 km/s, the H^+ temperature is 12 eV, and the heavy ion temperature is 95 eV. The number densities are 0.23, 0.23, and 0.65, leading to values of N_+ and N_M of 2.0 cm^{-3} and 24.9 amu/cm^3. In the top panel we show a fit assuming a composition of H^+, S^{3+}, and S^{2+}. The common speed is 177 km/s, the H^+ temperature is 20 eV, and the heavy ion temperature is 199 eV. The individual number densities are 0.28, 0.07, and 0.79, leading to values of N_+ and N_M of 2.0 cm^{-3} and 27.6 amu/cm^3.

It is clear from fits to the data depicted in Figures 24 and 27 that the assumption of only two heavy ion species in the L mode analysis drives up the fit temperature of the heavy ions to well above the true values. The fit tries to account for fluxes due to different A/Z^* values than those assumed by increasing the temperature of the assumed species. Attempts to fit more than two heavy ion species typically results in one of the densities being driven negative. This occurs because the densities are not constrained to be positive and the information content of the L mode spectra is low. However, in light of the M mode analysis of the 1537 UT spectrum, the fits to the L mode assuming two heavy ions do give us reasonable estimates of the total mass and charge densities, as well as the H^+ temperature, which is a reasonable indicator of the heavy ion temperatures. The best agreement with the M mode parameters comes from the assumption of H^+, S^{3+}, and O^+ for the

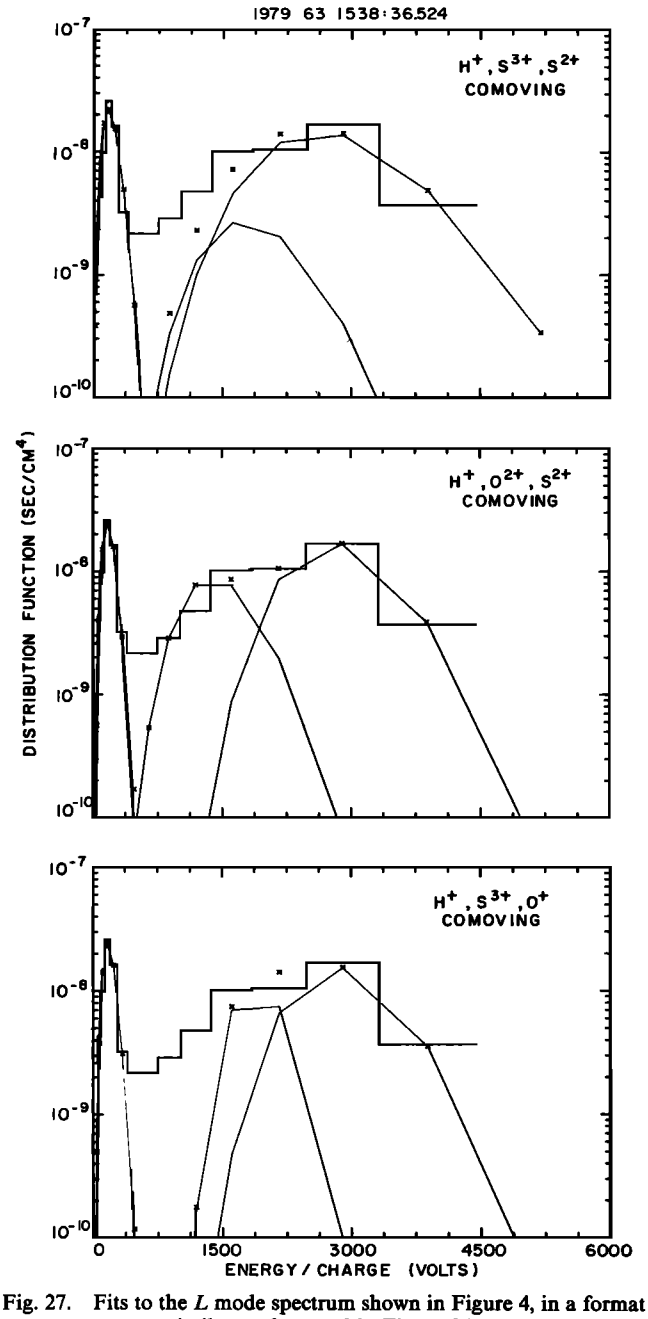

Fig. 27. Fits to the *L* mode spectrum shown in Figure 4, in a format similar to that used in Figure 24.

composition. More examples of *L* mode and *M* mode spectra and their analyses are given by *McNutt* [1980].

Acknowledgments. We are grateful to S. Olbert, J. D. Sullivan, F. Bagenal, J. Scudder, and E. Sittler for discussions and comments. We thank the magnetometer team (N. Ness, principal investigator) for access to magnetic field directions and magnitudes as necessary for the analysis of the plasma data. We would also like to acknowledge the cooperation of the computer operations staff at the MIT Laboratory for Nuclear Science. Special thanks are due to M. Terkoski, P. Milligan, and S. Skinner for help in preparation of the figures and to A. Bowes for preparation of the manuscript.

This work was supported under NASA contract 953733 to the Jet Propulsion Laboratory.

REFERENCES

Bagenal, F., and J. D. Sullivan, Spatial distribution of plasma in the Io torus, *Geophys. Res. Lett., 7,* 41, 1980.

Bagenal, F., and J. D. Sullivan, Direct plasma measurements in the Io torus and inner magnetosphere of Jupiter, *J. Geophys. Res.*, this issue.

Belcher, J. W., and R. L. McNutt, Jr., The dynamic expansion and contraction of the Jovian plasma sheet, *Nature, 287,* 813, 1980.

Belcher, J. W., C. K. Goertz, and H. S. Bridge, The low energy plasma in the Jovian magnetosphere, *Geophys. Res. Lett., 7,* 17, 1980.

Belcher, J. W., C. K. Goertz, J. D. Sullivan, and M. H. Acuña, Plasma observations of the Alfvén wave generated by Io, *J. Geophys. Res.*, this issue.

Binsack, J. H., Plasma studies with the IMP-2 satellite, Ph. D. thesis, pp. 41–44, Mass. Inst. of Technol., Cambridge, Aug. 1966.

Brice, N. M., and G. A. Ioannidis, The magnetospheres of Jupiter and earth, *Icarus, 13,* 173, 1970.

Bridge, H. S., J. W. Belcher, R. J. Butler, A. J. Lazarus, A. M. Mavretic, J. D. Sullivan, G. L. Siscoe, and V. M. Vasyliunas, The plasma experiment on the 1977 Voyager mission, *Space Sci. Rev., 21,* 259, 1977.

Bridge, H. S., J. W. Belcher, A. J. Lazarus, J. D. Sullivan, R. L. McNutt, Jr., F. Bagenal, J. D. Scudder, E. C. Sittler, G. L. Siscoe, V. M. Vasyliunas, C. K. Goertz, and C. M. Yeates, Plasma observations near Jupiter: Initial results from Voyager 1, *Science, 204,* 987, 1979*a*.

Bridge, H. S., J. W. Belcher, A. J. Lazarus, J. D. Sullivan, F. Bagenal, R. L. McNutt, Jr., K. W. Ogilvie, J. D. Scudder, E. C. Sittler, V. M. Vasyliunas, and C. K. Goertz, Plasma observations near Jupiter: Initial results from Voyager 2, *Science, 206,* 972, 1979*b*.

Broadfoot, A. L., M. J. S. Belton, P. Z. Takacs, B. R. Sandel, D. E. Shemansky, J. B. Hollberg, J. M. Ajello, S. K. Atreya, T. M. Donahue, H. W. Moos, J. L. Bertaux, J. E. Blamont, D. F. Strobel, J. C. McConnell, A. Dalgarno, R. Goody, and M. B. McElroy, Extreme ultraviolet observtions from Voyager 1 encounter with Jupiter, *Science, 204,* 979, 1979.

Brown, R. A., and F. H. Chaffee, Jr., High resolution spectra of sodium emission from Io, *Astrophys. J. Lett., 187,* L125, 1974.

Burke, B. F., and K. L. Franklin, Observations of a variable radio source associated with the planet Jupiter, *J. Geophys. Res., 60,* 213, 1955.

Burlaga, L. F., J. W. Belcher, and N. F. Ness, Disturbances observed near Ganymede by Voyager 2, *Geophys. Res. Lett., 7,* 21, 1980.

Connerney, J. E. P., M. H. Acuña, and N. F. Ness, Modeling the Jovian current sheet and inner magnetosphere, *J. Geophys. Res.*, this issue.

Davis, L., Jr., Stellar electromagnetic fields, *Phys. Rev., 72,* 632, 1947.

Davis, L., Jr., Stellar electromagnetic fields (abstract), *Phys. Rev., 73,* 536, 1948.

Ferraro, V. C. A., Non-uniform rotation of the sun and its magnetic field, *Mon. Not. R. Astron. Soc., 97,* 458, 1937.

Frank, L. A., K. L. Ackerson, J. H. Wolfe, and J. D. Mihalov, Observations of plasmas in the Jovian magnetosphere, *J. Geophys. Res., 81,* 457, 1976.

Goertz, C. K., Comments on 'Longitudinal asymmetry of the Jovian magnetosphere and the periodic escape of energetic particles,' by T. W. Hill and A. J. Dessler, *J. Geophys. Res., 81,* 5601, 1976.

Goertz, C. K., The Jovian magnetodisk, *Space Sci. Rev., 23,* 319, 1979.

Goertz, C. K., and M. F. Thomsen, Radial diffusion of Io-injected plasma, *J. Geophys. Res., 84,* 1499, 1979.

Gold, T., Motions in the magnetosphere of the earth, *J. Geophys. Res., 64,* 1219, 1959.

Goldstein, H., Theory of the plasma sheet in the Jovian magnetosphere, *Planet. Space Sci., 25,* 673, 1977.

Gurnett, D. A., F. L. Scarf, W. S. Kurth, R. R. Shaw, and R. L. Poynter, Determination of Jupiter's electron density profile from plasma wave observations, *J. Geophys. Res.*, this issue.

Hasegawa, A., Ballooning instability and plasma density limitations in Jovian magnetosphere, paper presented at Conference on Physics of the Jovian Magnetosphere, Rice Univ., Houston, Tex., 1980.

Hill, T. W., Interchange stability of a rapidly rotating magnetosphere, *Planet. Space Sci., 24,* 1151, 1976.

Hill, T. W., Inertial limit on corotation, *J. Geophys. Res., 84,* 6554, 1979.

Hill, T. W., Corotation lag in Jupiter's magnetosphere: Comparison of observation and theory, *Science, 207,* 301, 1980.

Hill, T. W., and F. C. Michel, Heavy ions from the Galilean satellites

and the centrifugal distortion of the Jovian magnetosphere, *J. Geophys. Res., 81,* 4561, 1976.

Ioannidis, G. A., and N. M. Brice, Plasma densities in the Jovian magnetosphere: Plasma slingshot or Maxwell demon?, *Icarus, 14,* 360, 1971.

Kaiser, M. L., and M. D. Desch, Narrow-band Jovian kilometric radiation: A new radio component, *Geophys. Res. Lett., 7,* 389, 1980.

Kennel, C. F., and F. V. Coroniti, Is Jupiter's magnetosphere like a pulsar's or earth's?, *Space Sci. Rev., 17,* 857, 1975.

Krimigis, S. M., T. P. Armstrong, W. I. Axford, C. O. Bostrom, C. Y. Fan, G. Gloeckler, L. J. Lanzerotti, E. P. Keath, R. D. Zwickl, J. F. Carbary, and D. C. Hamilton, Hot plasma environment at Jupiter: Voyager 2 results, *Science, 206,* 977, 1979.

Krimigis, S. M., J. F. Carbary, E. P. Keath, G. Gloeckler, W. I. Axford, L. J. Lanzerotti, and T. P. Armstrong, Characteristics of hot plasma in the Jovian magnetosphere: Results from the Voyager spacecraft, *J. Geophys. Res.,* this issue.

Kupo, I., Y. Mekler, and A. Eviatar, Detection of ionized sulfur in the Jovian magnetosphere, *Astrophys. J. Lett., 205,* L51, 1976.

McDonald, F. B., A. W. Schardt, and J. H. Trainor, Energetic protons in the Jovian magnetosphere, *J. Geophys. Res., 84,* 2579, 1979.

McNutt, R. L., Jr., The dynamics of the low energy plasma in the Jovian magnetosphere, Ph. D. thesis, Dep. of Phys., Mass. Inst. of Technol., Cambridge, July 1980.

McNutt, R. L., Jr., J. W. Belcher, J. D. Sullivan, F. Bagenal, and H. S. Bridge, Departure from rigid corotation of plasma in Jupiter's dayside magnetosphere, *Nature, 280,* 803, 1979.

Melrose, D. B., Rotational effects on the distribution of thermal plasma in the magnetosphere of Jupiter, *Planet. Space Sci., 15,* 381, 1967.

Mendis, D. A., and W. I. Axford, Satellites and magnetospheres of the planets, *Annu. Rev. Earth Planet. Sci., 2,* 419, 1974.

Ness, N. F., M. H. Acuña, R. P. Lepping, L. F. Burlaga, K. W. Behannon, and F. M. Neubauer, Magnetic field studies at Jupiter by Voyager 1: Preliminary results, *Science, 204,* 982, 1979*a*.

Ness, N. F., M. H. Acuña, R. P. Lepping, L. F. Burlaga, K. W. Behannon, and F. M. Neubauer, Magnetic field studies at Jupiter by Voyager 2: Preliminary results, *Science, 206,* 966, 1979*b*.

Neugebauer, M., and A. Eviatar, An alternative interpretation of Jupiter's 'plasmapause,' *Geophys. Res. Lett., 3,* 708, 1976.

Northrop, T. G., T. J. Birmingham, and A. W. Schardt, Anisotropies in the fluxes of Pioneer 10 protons, *J. Geophys. Res., 84,* 47, 1979.

Olbert, S., Summary of experimental results from the MIT detector on IMP-1, in *Physics of the Magnetosphere,* vol. 10 edited by R. L. Carovillano, p. 641, D. Reidel, Hingham, Mass., 1968.

Piddington, J. H., and J. F. Drake, Electrodynamic effects of Jupiter's satellite Io, *Nature, 217,* 935, 1968.

Scudder, J. D., E. C. Sittler, Jr., and H. S. Bridge, A survey of the plasma electron environment of Jupiter: A view from Voyager, *J. Geophys. Res.,* this issue.

Siscoe, G. L., On the equatorial confinement and velocity space distribution of satellite ions in Jupiter's magnetosphere, *J. Geophys. Res., 82,* 1641, 1977.

Siscoe, G. L., and D. Summers, Centrifugally driven diffusion of Iogenic plasma, *J. Geophys. Res.,* this issue.

Sittler, E. C., Studies of the electron component of the solar wind and magnetospheric plasma, Ph.D. thesis, p. 56, Mass. Inst. of Technol., Cambridge, Feb. 1978.

Smith, E. J., L. Davis, Jr., D. E. Jones, P. J. Coleman, Jr., D. S. Colburn, P. Dyal, C. P. Sonett, and A. M. A. Frandsen, The planetary magnetic field and magnetosphere of Jupiter: Pioneer 10, *J. Geophys. Res., 79,* 3501, 1974.

Smith, E. J., L. Davis, Jr., D. E. Jones, P. J. Coleman, Jr., D. S. Colburn, P. Dyal, and C. P. Sonett, Jupiter's magnetic field, magnetosphere, and interaction with the solar wind: Pioneer 11, *Science, 188,* 451, 1975.

Sullivan, J. D., and F. Bagenal, *In situ* identification of various ionic species in Jupiter's magnetosphere, *Nature, 280,* 798, 1979.

Van Allen, J. A., D. N. Baker, B. A. Randall, and D. D. Sentman, The magnetosphere of Jupiter as observed with Pioneer 10, 1, Instrument and principle findings, *J. Geophys. Res., 79,* 3559, 1974.

Vasyliunas, V. M., Deep space plasma measurements, in *Methods of Experimental Physics,* vol. 9B of *Plasma Physics,* edited by R. H. Lovbergs, p. 49, Academic, New York, 1971.

Walker, R. J., M. G. Kivelson, and A. W. Schardt, High β plasma in the dynamic Jovian current sheet, *Geophys. Res. Lett., 5,* 799, 1978.

Warwick, J. W., J. B. Pearce, A. C. Riddle, J. K. Alexander, M. D. Desch, M. L. Kaiser, J. R. Thieman, T. D. Carr, S. Gulkis, A. Boischot, C. C. Harvey, and B. M. Pedersen, Voyager 1 planetary radio astronomy observations near Jupiter, *Science, 204,* 995, 1979.

(Received July 28, 1980;
revised October 27, 1980;
accepted October 28, 1980.)